Identification of Hippocampus-Related Candidate Genes for Alzheimer's Disease

Keiko Taguchi, MD,[1] Hidehisa D. Yamagata, MD, PhD,[2] Wangtao Zhong, MD,[1] Kouzin Kamino, MD, PhD,[3] Hiroyasu Akatsu, MD, PhD,[4] Ryuji Hata, MD, PhD,[5] Takayuki Yamamoto, MD, PhD,[4] Kenji Kosaka, MD, PhD,[4] Masatoshi Takeda, MD, PhD,[3] Ikuko Kondo, MD, PhD,[2] and Tetsuro Miki, MD, PhD[1]

Alzheimer's disease (AD) is a complex multifactorial disease in which many genetic and environmental factors are involved. We performed an association study using 376 AD patients and 376 control subjects. We studied 35 single nucleotide polymorphisms in 35 genes that were significantly downregulated or upregulated only in the AD hippocampus compared with control and found that 9 single nucleotide polymorphisms were associated with AD. Our data indicated that single nucleotide polymorphisms could highly reflect differences in gene expression. Furthermore, an intronic polymorphism (+9943T/C) in *POU2F1* was most significantly associated with AD (p = 0.0007). Our results suggest that *POU2F1* is a candidate gene for AD.

Ann Neurol 2005;57:585–588

Alzheimer's disease (AD; MIM #104300) is a neurodegenerative disorder characterized by progressive memory impairment and multiple cognitive deficits in mid to late life.[1] Its pathological hallmarks consist of neuritic plaques and neurofibrillary tangles in the cerebral cortex, accompanied by neuronal loss.[2–4] These neuropathological findings are prominent in the temporal neocortex and hippocampus. To date, four genes have been established to be associated with AD phenotypes, including the amyloid precursor protein gene, apolipoprotein E (*ApoE*) gene, and presenilin 1 (*PSEN1*) and presenilin 2 (*PSEN2*) genes.[5] The majority of familial AD cases are associated with *PSEN1* mutations, and the majority of sporadic cases are related to *ApoE-ε4*.[6–8] It has become clear that genetic and environmental factors are involved in the pathophysiology of this disease, but it remains unclear how these factors combine and ultimately lead to the neurodegenerative process.[1,2]

Recent advances in molecular biological technology have demonstrated that single nucleotide polymorphisms (SNPs) are a valuable tool for investigating the genetic basis of disease. SNPs may be used in not only positional cloning studies, but also genome-wide association studies.[9] Previously, we reported significantly upregulated or downregulated gene expression in the AD hippocampus using a complementary DNA microarray.[10] The most upregulated gene proved to be calcineurin Aβ (*PPP3CB*). We made a list of the top 20 named genes upregulated or downregulated (Table 1). Because SNPs may themselves represent genetic variants that affect disease susceptibility or progression, evaluating variants in a disease-associated gene is of great importance to identify alleles responsible for disease susceptibility or progression.

Subjects and Methods

Subjects

The Ethics Committee of Ehime University School of Medicine approved the study protocol. Patients were selected using National Institute of Neurological and Communication Disorders-Alzheimer's Disease and Related Disorders Association criteria for definite or probable AD, and nondemented control subjects were rigorously evaluated for cognitive impairment using the Mini-Mental State Examination.[3,11] Brain and blood samples were obtained with informed consent from the patients (or their guardians) in the Chubu, Kansai, and Ehime areas of Japan. A total of 376 unrelated AD patients had been diagnosed previously, and 376 control subjects (outpatients or healthy volunteers) were selected and matched for age and place of residence with each patient. The mean age ± SD at the time of this study was 78.2 ± 8.3 years for late-onset AD and 75.5 ± 4.9 years for control subjects. The female proportion was greater in the AD group (70.5%) than in the control group (54.7%). Genomic DNA was purified by standard procedures from lymphocytes, lymphoblastoid cell lines, or brain samples.[12]

We compared allele frequencies between sporadic late-onset AD and healthy control subjects. Because *ApoE-ε4* is a risk factor for AD, we stratified the population by ε4 carrier status. *ApoE* genotyping was performed as described previously. Allelic and genotypic distributions were analyzed by the usual χ^2 test of association. The genotypic frequencies were compared by χ^2 test with the values predicted by the assumption of Hardy–Weinberg equilibrium in the sample. p values less than 0.05 were considered significant. Odds ratios (ORs) were calculated with two-tailed p values and 95%

From the Departments of [1]Geriatric Medicine and [2]Medical Genetics, Ehime University School of Medicine, National University Corporation, Ehime; [3]Division of Psychiatry and Behavioral Proteomics, Department of Post-Genomics and Diseases, Osaka University Graduate School of Medicine, Suita; [4]Choju Medical Institute, Fukushimura Hospital, Toyohashi; and [5]Division of Functional Histology, Ehime University School of Medicine, National University Corporation, Ehime, Japan.

Received Nov 22, 2004, and in revised form Jan 13, 2005. Accepted for publication Jan 24, 2005.

Published online Mar 28, 2005 in Wiley InterScience (www.interscience.wiley.com). DOI: 10.1002/ana.20433

Address correspondence to Dr Yamagata, Department of Medical Genetics, Ehime University School of Medicine, National University Corporation, Touon-shi, Ehime 791-0295, Japan.
E-mail: hideyama@m.ehime-u.ac.jp

Table 1. List of 17 (or 18) Genes of Top 20 Genes and SNPs Significantly Up-Regulated or Down-Regulated in Hippocampus from AD Brain but not Control Brain (Chromosomal Location)

Up-Regulated Genes	Down-Regulated Genes
PPP3CB (10q22); calcineurin A beta; rs12644	*HMMR* (5q34); hyaluronan-mediated motility receptor; rs299290
RANBP1 (22q11); RAN binding protein 1; hCV2613312	*LAMB1* (7q31); laminin, beta 1; rs2237685
GNA11 (19p13); guanine nucleotide binding protein 11; rs308064	*POU2F1* (1q24.2); POU domain, class 2, transcription factor 1; rs1407814
CSN1 (4q13); casein, alpha; rs2279526	*MYH8* (17p13); myosin, heavy polypeptide 8, skeltal muscle; rs2024076
FCER1G (1q23); Fc fragment of IgE, high affinity 1; rs11421	*TM4SF5* (17p13); transmembrane 4 superfamily member 1; rs3851
ART3 (4q21); ADP-ribosyltransferase 3; hCV450363	*ADORA2B* (17p12); adenosine A2b receptor; rs1076424
FGL2 (7q11); fibrinogen-like 2; rs2075761	*COL11A1* (1p21.1); collagen, type XI alpha; rs3753841
ZAP128 (14q24.3); peroxisomal long-chain acyl-CoA thioesterase; hCV11164654	*PDCD11* (10q24.33); human mRNA for KIAA0185 gene; rs2986014
CLCNKB (1p36); chloride channel, kidney, B; hCV1814709	*TGM4* (3p21); transglutaminase 4; rs1995641
MCM3AP (21q22); minichromosome maintenance 3-associated protein; rs3788252	*PCK2* (14q11.2); phosphoenolpyruvate carboxykinase 2; rs2071586
FACL4 (Xq23); fatty acid CoA ligase, long chain 4; rs1324805	*HSPC242* (22q12); Homo sapiens PAC clone DJ130H16; rs2072158
RPS15 (19p13.3); ribosomal protein S15; rs1847602	*LCK* (1p35); lymphocyte-specific protein tyrosine kinase; hCV1895446
GBP2 (1p22); guanylate binding protein 2, interferon-inducible; rs4656097 (hCV2431431)	*TNFRSF8* (1p36); tumor necrosis factor receptor superfamily, member 8; hCV9567
PHKG2 (16p11.2); phosphorylase kinase, gamma 2; hCV27530858	*DPYS* (8q22); dihydropyrimidinase; rs2246815
AVPR1A (12q14.2); arginine vasopressin receptor 1A; rs1042615	*EGR2* (10q21.3); early growth response 2; rs2297489
PSMB7 (9q33.3); proteasome subunit, beta-type 7; hCV3112402	*CD36* (7q21); CD36 antigen; rs1358337
EFEMP1 (2p16); EGF-containing fibulin-like extracellular matrix protein 1; rs1344733	*CAV2* (7q31); caveolin 2; rs2270189
	AKAP8 (19p13.12); A kinase anchor protein 95; hCV2596739

confidence intervals (CIs). Bonferroni correction was applied to reduce type I error. The relation of genotypic factors and the effect of *ApoEε4* to AD was assessed with logistic regression analysis. Statistical analyses were performed with SPSS software version 11.0 (SPSS, Chicago, IL).

Genotyping

We selected 35 among 40 genes due to the available database; 18 genes were significantly downregulated and 17 genes were significantly upregulated in the AD hippocampus compared with control according to our previous report (see Table 1). We performed a genotype of one SNP in each of the 35 candidate genes. The selected SNPs met the following criteria. First, the polymorphism was confirmed in the Japanese population. Second, the minor allele frequency was between 0.1 and 0.5 according to common disease–common variant hypothesis.[13] Third, the variant may potentially influence gene expression (eg, promoter, exon, missense, and so forth). Intronic SNPs in the strong linkage disequilibrium block around the promoter region. Fourth, a TaqMan probe was available. Genotyping of SNPs was performed using the TaqMan-polymerase chain reaction method. Amplification was performed according to the manufacturer's protocol. The fluorescence intensity of the polymerase chain reaction products was measured using an ABI PRISM 7900HT Sequence Detection System (Applied Biosystems, Foster City, CA).

Results

Two (*CAV2, RANBP1*) of 35 SNPs were not polymorphic in our samples (data not shown). We analyzed the data for the remaining 33 SNPs. The distribution obtained for the patients and control subjects almost reached Hardy–Weinberg equilibrium.

Of 17 SNPs with downregulated gene expression tested, 5 (*POU2F1, MYH8, CD36, DPYS, COL11A1*) showed a significant association with AD. Of 16 SNPs with upregulated gene expression, 4 (*GNA11, FCER1G, MCM3AP, GBP2*) showed a significant association with AD. The genotypic and allelic distributions of each SNP in the patients and control subjects are shown in Table 2.

Among them, we found a strong association between the *POU2F1* +9943T/C polymorphism and AD ($p = 0.0007$; $p = 0.023$ after Bonferroni correction). The allelic frequency for *POU2F1* +9943T was 0.09 in control subjects and 0.15 in AD patients. After the logistic regression analysis, a recessive model provided the

Table 2. Genotype and Allele Numbers of Nine SNPs Significantly Associated with AD Risk

	Gene Name	rs number	Celera	Location		AD : Control (Genotype)	*P* value	AD : Control (allele)	*P* value	OR (95% CI) APOE4(−) Subjects
Down-regulated	*POU2F1*	rs1407814	hCV1622428	intron 2	9943T/C	TT/TC/CC = 11/90/275 : 2/65/309	0.0022**	T/C = 112/640 : 69/683	0.0007**	1.73 (1.11–2.69)
	MYH8	rs2024076	hCV2179107	intron 18	13583T/C	TT/TC/CC = 9/132/235 : 23/110/243	0.017*	T/C = 150/602 : 156/596	0.700	1.98 (0.78–5.06)
	CD36	rs1358337	hCV1803785	intron 3	12329A/G	GG/GA/AA = 44/152/180 : 51/182/143	0.024*	G/A = 240/512 : 284/468	0.017*	1.35 (0.79–2.29)
	DPYS	rs2246815	hCV9595720	intron 5	38687A/G	GG/GA/AA = 174/163/39 : 137/192/47	0.023*	G/A = 511/241 : 466/286	0.015*	1.45 (0.80–2.64)
	COL11A1	rs3753841	hCV2947954	exon 52	193817A/G	AA/AG/GG = 178/160/38 : 158/156/62	0.030*	A/G = 516/236 : 472/280	0.017*	1.62 (0.95–2.75)
Up-regulated	*GNA11*	rs308064	hCV3149364	intron 2	18527T/C	TT/TC/CC = 144/176/56 : 156/186/34	0.046*	T/C = 464/288 : 498/254	0.068	1.02 (0.70–1.46)
	FCER1G	rs11421	hCV1841966	exon 5	3825T/C	TT/TC/CC = 132/159/85 : 140/183/53	0.009**	T/C = 423/329 : 463/289	0.036*	1.05 (0.73–1.52)
	MCM3AP	rs3788252	hCV3270916	intron 25	43966T/C	TT/TC/CC = 18/144/214 : 31/115/230	0.026*	T/C = 180/572 : 177/575	0.856	1.19 (0.83–1.71)
	GBP2	rs4656097	hCV2431431	intron 6	6000T/A	TT/TA/AA = 17/155/204 : 22/122/232	0.041*	T/A = 189/563 : 166/586	0.162	1.14 (0.84–1.54)

*P < 0.05, **P < 0.01, OR: odds ratio, 95% CI: confidence interval.

best fit ($p = 0.020$; OR, 6.33; 95% CI, 1.33–30.0), but a dominant model could not be rejected ($p = 0.070$; OR, 1.42; 95% CI, 1.42–2.08). We then examined the TT genotype as a risk factor for AD, considering the *ApoE* status. To quantify possible interactions between *ApoE-ε4* and *POU2F1*, we analyzed the data with respect to various carrier status combinations, taking subjects who had neither *ApoE-ε4* nor *POU2F1* as a reference (Table 3). Four categories were defined by the presence (+) or absence (−) of an ε4 or TT genotype. As expected, *ApoE-ε4* conferred an increased risk for AD (OR, 5.09; 95% CI, 3.61–7.18). The TT genotype alone showed an increased risk (OR, 1.73; 95% CI, 1.11–2.69), and the OR for *ApoE-ε4* and the TT genotype was 6.08. As for the interaction between the ApoE-ε4 and *POU2F1-T* alleles for the risk for AD, logistic regression analysis did not indicate a significant effect ($p = 0.30$). The synergetic effect of TT allele in patients having *ApoE-ε4* was weak. The other eight gene SNPs did not show significant associations in the *ApoE-ε4* (−) subjects (see Table 2).

Discussion

In this study, we hypothesized that genes demonstrating significant differences in expression level between AD and control hippocampus might play a potential role as disease modifiers or disease susceptibility genes. To confirm this assumption, we performed an association study using these AD candidate genes. Consequently, we found 9 significant associations in 33 SNPs (genes). Compared with general association studies, the detection rate of positive SNPs (genes) in this study was markedly high. Our data indicated that SNPs could highly reflect difference in gene expression.

Previously, we reported a comparison of the gene expression in the hippocampus containing neurofibrillary tangle–associated lesions from an AD patient with that in the parietal cortex from the same patient, which lacked those lesions. Compared with control brain, the genes significantly upregulated or downregulated only in the AD brain were determined. The most upregulated gene proved to be calcineurin Aβ (*PPP3CB*), although its SNP showed no association (allele: $p = 0.51$; genotype: $p = 0.81$). Our analysis showed that 5 of 17 SNPs with downregulated gene expression (*POU2F1, MYH8, CD36, DPYS, COL11A1*) were associated with AD, and 4 of 16 SNPs with upregulated gene expression (*GNA11, FCER1G, MCM3AP, GBP2*) were associated with AD.

Among them, the POU domain, class 2, transcription factor 1 (POU2F1; also called Oct-1) showed the strongest association with AD. *POU2F1*, a member of the POU family transcription factors, is ubiquitously expressed in both the embryo and the adult.[14] *POU2F1* also takes a part in regulation of cell type–specific gene expression. It regulates some genes in the immune system including those encoding light and heavy chains of immunoglobulins, IL-2, IL-3, IL-5, IL-8, granulocyte/macrophage colony stimulating factor, and CD20.[15] Furthermore, an alternatively spliced variant of human *POU2F1* is only expressed in lymphoid tissues and brain.[15]

Our data suggest that *POU2F1* mediates immune and inflammatory responses in the AD brain. In fact, increasing evidence suggests that the immune system may play an important role in the degenerative process of AD.[16] The +9943T allele was significantly associated with AD in individuals lacking an ApoE-ε4 allele. Therefore, *POU2F1* (1q24.2) is an additional risk factor, synergistic with the *ApoE* gene. According to the SNPbrowser Version 2.0 (Applied Biosystems), strong linkage disequilibrium is shown around the *POU2F1* gene. Therefore, it is reasonable to think that +9943T/C polymorphism in intron 2 can contribute

Table 3. Relative Risks for Interaction Between APOEε4 and +9943T in POU2F1

		AD Cases	Controls	Odds Ratio	95%CI		AD Cases	Controls	Odds Ratio	95%CI
	9943T/C									
	non-TT	365	374	Reference	—	APOEε4 −	193	317	Reference	—
	TT	11	2	5.64	1.24–25.6	+	183	59	5.09	3.61–7.18
APOEε4	9943T									
−	−	145	266	Reference	—					
−	+	48	51	1.73	1.11–2.69					
+	−	130	43	5.55	3.72–8.27					
+	+	53	16	6.08	3.35–11.0					

APOEε4 (+), one or two copies of ε4: APOEε4 (−), no copies of ε4, 95% CI: confidence interval.

to promoter activity. +9943T/C may be the representative marker that influences gene expression. Our data suggest that these nine genes are susceptibility genes of sporadic AD. This should be examined further by functional analysis of the nine gene polymorphisms. Also, extensive investigations using different SNPs in the same genes, different populations, and a larger sample size are required to clarify the role of the nine gene polymorphisms.

This work was supported by grants from the Japanese Millennium Project (00L 01413, M.T.), the Japan Society for the Promotion of Science and the Novartis Foundation for the Gerontological Research (H.D.Y.).

We are grateful to all participants in this study.

References

1. Kawas CH, Katzman R. The epidemiology of dementia and Alzheimer disease. In Terry RD, Katzman R, Bick KL, et al, eds. Alzheimer disease. Philadelphia: Lippincott Williams & Wilkins, 1999:95–116.
2. Selkoe DJ. Alzheimer's disease: genes, proteins, and therapy. Physiol Rev 2001;81:741–766.
3. McKhann G, Drachman D, Folstein M, et al. Clinical diagnosis of Alzheimer's disease: report of the NINCDS-ADRDA Work Group under the auspices of Department of Health and Human Services Task Force on Alzheimer's disease. Neurology 1984;34:939–944.
4. Bird TD, Sumi SM, Nemens EJ, et al. Phenotypic heterogeneity in familial Alzheimer's disease: a study of 24 kindreds. Ann Neurol 1989;25:12–25.
5. Campion D, Flaman JM, Brice A, et al. Mutations of the presenilin gene in families with early-onset Alzheimer's disease. Hum Mol Genet 1995;4:2373–2377.
6. Strittmatter WJ, Saunders AM, Schmechel D, et al. Apolipoprotein E: high-avidity binding to beta-amyloid and increased frequency of type 4 allele in late-onset familial Alzheimer's disease. Proc Natl Acad Sci U S A 1993;90:1977–1981.
7. van Duijn C, de Knijff P, Cruts M, et al. Apolipoprotein E4 allele in a population-based study of early-onset Alzheimer's disease. Nat Genet 1994;7:74–78.
8. Houlden H, Crook R, Backhovens H, et al. ApoE genotype is a risk factor in nonpresenilin early-onset Alzheimer's disease families. Am J Med Genet 1998;81:117–121.
9. Erichsen HC, Chanock SJ. SNPs in cancer research and treatment. Br J Cancer 2004;90:747–751.
10. Hata R, Masumura M, Akatsu H, et al. Up-regulation of calcineurin Abeta mRNA in the Alzheimer's disease brain: assessment by cDNA microarray. Biochem Biophys Res Commun 2001;284:310–316.
11. Folstein MF, Folstein SE, McHugh PR. Mini-Mental state: a practical method for grading the cognitive state of patients for the clinician. J Psychiatr Res 1975;12:189–198.
12. Sambrook J, Fritsch EF, Maniatis T. Molecular cloning: a laboratory manual. 2nd ed. New York: Cold Spring Harbor Laboratory Press, 1989:9–14.
13. Doris PA. Hypertension genetics, single nucleotide polymorphisms, and the common disease: common variant hypothesis. Hypertension 2002;39:323–331.
14. Ryan AK, Rosenfeld MG. POU domain family values: flexibility, partnerships, and developmental codes. Genes Dev 1997; 11:1207–1225.
15. Luchina NN, Krivega IV, Pankratova EV. Human Oct-1L isoform has tissue-specific expression pattern similar to Oct-2. Immunol Lett 2003;85:237–241.
16. Monsonego A, Weiner HL. Immunotherapeutic approaches to Alzheimer's disease. Science 2003;302:834–838.

Acta Neuropathol (2005)
DOI 10.1007/s00401-005-0004-1

ORIGINAL PAPER

Hiroshige Fujishiro · Hiroyuki Umegaki
Daisuke Isojima · Hiroyasu Akatsu · Akihisa Iguchi
Kenji Kosaka

Depletion of cholinergic neurons in the nucleus of the medial septum and the vertical limb of the diagonal band in dementia with Lewy bodies

Received: 31 July 2005 / Revised: 19 September 2005 / Accepted: 19 September 2005

Abstract The cholinergic basal forebrain is divided into four subregions (Ch1–4), and cholinergic neuronal loss in the nucleus basalis of Meynert (Ch4) has been correlated with cognitive impairments in both Alzheimer's disease (AD) and dementia with Lewy bodies (DLB). However, the Ch1–2 regions, which provide the major cholinergic innervation to the hippocampus, have not been investigated in DLB. The purpose of this study was to reveal the cholinergic neuronal changes in the medial septum (Ch1) and the nucleus of the vertical limb of the diagonal band (Ch2) of DLB brains. Using choline acetyltransferase (ChAT) immunohistochemistry, we showed that the number of ChAT-immunoreactive neurons in DLB brains was significantly lower than the numbers in AD and non-demented (control) brains. No significant difference in the number of ChAT-immunoreactive neurons was found between the AD and control brains. Moreover, the size of the ChAT-immunoreactive neurons was significantly smaller in the AD and DLB brains than in the control brains. These results show that cholinergic neurons of the Ch1-2 regions are more severely affected in DLB than in AD. Our DLB cases did not fulfill the neuropathologic criteria for definite AD. Furthermore, some Lewy bodies were observed in the Ch1-2 regions. Thus, cholinergic neuronal loss in the Ch1-2 regions might be specific to the pathology of DLB. Taking the distribution of cholinergic fibers in the hippocampus into consideration, this study suggests a possibility that hippocampal cholinergic projection is involved in Lewy-related neurites in the CA2–3 regions, the origin of which remains unclear.

Keywords Septal nuclei · Basal forebrain · Immunohistochemistry · Choline acetyltransferase · Cholinesterase inhibitor

H. Fujishiro (✉) · H. Umegaki · A. Iguchi
Department of Geriatrics, Medicine in Growth and Aging, Program in Health and Community Medicine, Nagoya University Graduate School of Medicine, 65 Tsurumai-cho, Showa-ku, 466-8550, Nagoya, Japan
E-mail: fujishi@med.nagoya-u.ac.jp

D. Isojima · H. Akatsu · H. Fujishiro
Choju Medical Institute, Fukushimura Hospital, 19-16 Noyori-cho, Aza-yamanaka, 441-8124, Toyohashi, Japan

K. Kosaka · D. Isojima
Department of Psychiatry, Yokohama City University, 3-9 Fukuura, Kanazawa-ku, 236-0004, Yokohama, Japan

Introduction

Dementia with Lewy bodies (DLB) is the second most frequent neurodegenerative dementing disorder after Alzheimer's disease (AD) [1, 18]. Hippocampal pathology is important in DLB as well as AD, since memory impairment, a chief symptom of both the disorders, is closely related to degeneration of the hippocampus. Lewy-related neurites are usually observed in the CA2–3 regions of the hippocampus in DLB [6, 7, 9, 11, 18], whereas these regions are relatively preserved in AD. In addition, immunoelectron microscopic examinations have revealed that these Lewy-related neurites are distal axons that have undergone change. These neurites are partially immunostained with a neurofilament antibody, but not with a tyrosine hydroxylase antibody [7]. Although the origin of Lewy-related neurites has been poorly understood, the absence of the degenerating axon terminals in hippocampal regions other than the CA2–3 regions of DLB brains might indicate that this pathology is associated with impairments of the hippocampal projection.

Cholinergic neurons in the basal forebrain form a cholinergic column comprising the medial septum, the nucleus of the diagonal band, and the nucleus basalis of Meynert. Mesulam et al. proposed the nomenclature of Ch1 through 4 to designate the various subdivisions of the basal forebrain cholinergic neurons [19]. The medial septum (Ch1) and the vertical limb of the nucleus of the diagonal band (Ch2) provide the cholinergic innervation of the hippocampal formation, and the nucleus basalis

(Ch4) projects to the amygdaloid nuclei and the cerebral cortex [15, 22]. Choline acetyltransferase (ChAT) activity in the cerebral cortex, a decrease in which is correlated with neuronal loss in the nucleus basalis of Meynert (Ch4), has been reported to be involved in cognitive function [16]. Moreover, the reduction of the neocortical presynaptic cholinergic inputs is more severe in DLB brains than in AD brains. Therefore, cholinesterase inhibitors are thought to be more effective in DLB patients than in AD patients [2, 10, 26]. On the other hand, cholinergic neurons within the hippocampal projecting nuclei of the Ch1–2 regions are minimally affected in AD brains as compared with non-demented brains [21, 23]. These neurons have not yet been investigated in DLB brains.

A previous study of ChAT-like immunoreactivity in hippocampal formation in humans showed that punctuate ChAT-immunostaining was conspicuous in the stratum pyramidale of the CA2–3 regions [27]. In the current study, we hypothesized that the Ch1–2 cholinergic neurons projecting to the hippocampus are involved in hippocampal CA2–3 pathology. To test this hypothesis, we performed a qualitative and semiquantitative ChAT-immunohistochemical analysis of cholinergic neurons over the entire length of the Ch1–2 regions of DLB brains, AD brains and non-demented control brains, and compared the results.

Materials and methods

Subjects

Fifteen autopsied brains from eight DLB cases (DLB group: mean age, 75.0 ± 12.6 years; mean brain weight, 1,200 ± 119 g), four AD cases (AD group: mean age, 83.5 ± 0.5 years; mean brain weight, 1,090 ± 43 g) and three non-demented control cases (control group: mean age, 83.3 ± 3.5 years; mean brain weight, 1,145 ± 123 g) were examined in the present study. DLB was diagnosed based on the neuropathological criteria of DLB and divided into five limbic types and three neocortical types [18]. Four AD cases fulfilled the neuropathological criteria of AD according to the NIA-RI-criteria [31]. The progression of Alzheimer pathology was classified from stages 1 to 6 by Braak staging [4]. Neither the DLB group nor the control group fulfilled the pathological criteria for AD [17, 31]. No significant difference was found in mean age or mean brain weight among the three groups. The mean values of the final mini-mental state examination (MMSE) cognitive score before death were also compared between the DLB group and AD group [8], and no significant difference was found (mean MMSE for the DLB group: 4.5 ± 4.7; for the AD group: 4.0 ± 8.0). Informed written consent was obtained from the patients' guardians before carrying out the dissection, and study design was approved by the ethics committee of the Choju medical institute.

Immunocytochemistry

Tissue blocks including the septal nucleus and the vertical limb of the diagonal band were fixed in 4% paraformaldehyde in 0.1 M phosphate buffer (pH 7.4), embedded in paraffin and cut into serial coronal 7-μm-thick sections. The region studied extended from the anterior border of the septal nucleus to the anterior commissure. Sections taken every 280 μm, i.e., every 40th section were stained with hematoxylin-eosin (HE). By this method, we could examine the entire medial septal nucleus and vertical limb of the diagonal band. After the limits were decided, serial sections (seven to ten sections for each brain) were pretreated with 0.1% trypsin diluted with 0.1% $CaCl_2$ for 20 min, and then immunostained with polyclonal goat anti-ChAT antibody (1:100; Chemicon, Temecula, CA, USA) and monoclonal mouse anti-phosphorylated α-synuclein antibody (1:1,000; Wako, Tokyo, Japan) overnight at 4°C. Alfa-synuclein-immunostaining was performed to confirm the presence of Lewy bodies in the Ch1–2 regions in cases where bodies were observed by HE staining. These primary antibodies were diluted with phosphate-buffered saline (PBS) containing 3% normal goat serum. After incubation with the primary antibodies, the sections were treated with biotinylated secondary antibodies for 2.5 h at room temperature, followed by incubation in avidin-biotinylated horseradish peroxidase (HRP) complex (ABC Elite Kit; Vector, Burlingame, CA, USA) for 0.5 h at room temperature. Immunolabeling was visualized with 3,3′-diaminobenzidine (DAB; Dojindo, Kumamoto, Japan) and nickel ammonium sulfate. Before α-synuclein immunostaining, sections were pretreated with 98% formic acid for 3 min. To investigate the AD pathology in the Ch1–2 regions, the sections from all the brains were also stained by the Gallyas–Braak method.

Semiquantitative analysis of ChAT-immunoreactive neurons

ChAT-immunoreactive neurons in the Ch1–2 regions were semiquantitatively analyzed to investigate the depletion of cholinergic neurons. The number of ChAT-immunoreactive neurons was counted on each section by the two investigators (H.F. and D.I.) who were blinded to the groups. The assessments were repeated and any discrepancies between the evaluations of the two raters were resolved through discussion. The numbers of ChAT-immunoreactive neurons on each of the serial sections at 280 μm intervals were summed, and this value served as a substitute for the total number of neurons in each case.

Densitometric analysis of ChAT-immunoreactive neurons

ChAT-immunoreactivity was investigated by densitometric analysis to detect the depletion of cholinergic

activity in each neuron. The sections were examined under an Olympus microscopy with Olympus AX80T at a total magnification of 200 times. All of the digital images of ChAT-immunoreactive neurons were converted to grayscale using Photoshop 4.0J image processing software (Adobe Systems, Tokyo, Japan) and the image analysis was performed using Scion Image Beta software, Version 4.02 (Scion, Frederick, MD, USA) to determine the pixel density of ChAT-positive cells at a given threshold level. In the present study, the pixel counts of the ChAT-positive neurons determined by image analysis served as a substitute for the cell surface measurement in each neuron. ChAT-immunoreactive neurons in the Ch2 region were randomly selected and the cell surface measurement was performed (pixels/cell). The average cell surface value was calculated for 100 neurons in each brain, followed by the average cell surface value for each of three groups.

Statistical analysis

The data are expressed as the mean ± SEM. The Kruskal–Wallis test followed by the Mann–Whitney *U*-test was used to compare differences among the three groups. p values below 0.05 were considered statistically significant. All statistical analysis was performed using StatView software (Version 5.0) for Windows.

Results

ChAT-immunoreactive neurons were observed from the medial septum (Ch1) to the nucleus of the vertical limb of the diagonal band (Ch2) in all cases. The Ch2 merges with the caudal portions of the Ch1; the Ch2 is located ventral to the decussation of the anterior commissure and reaches the posterior edge of the ventral striatum.

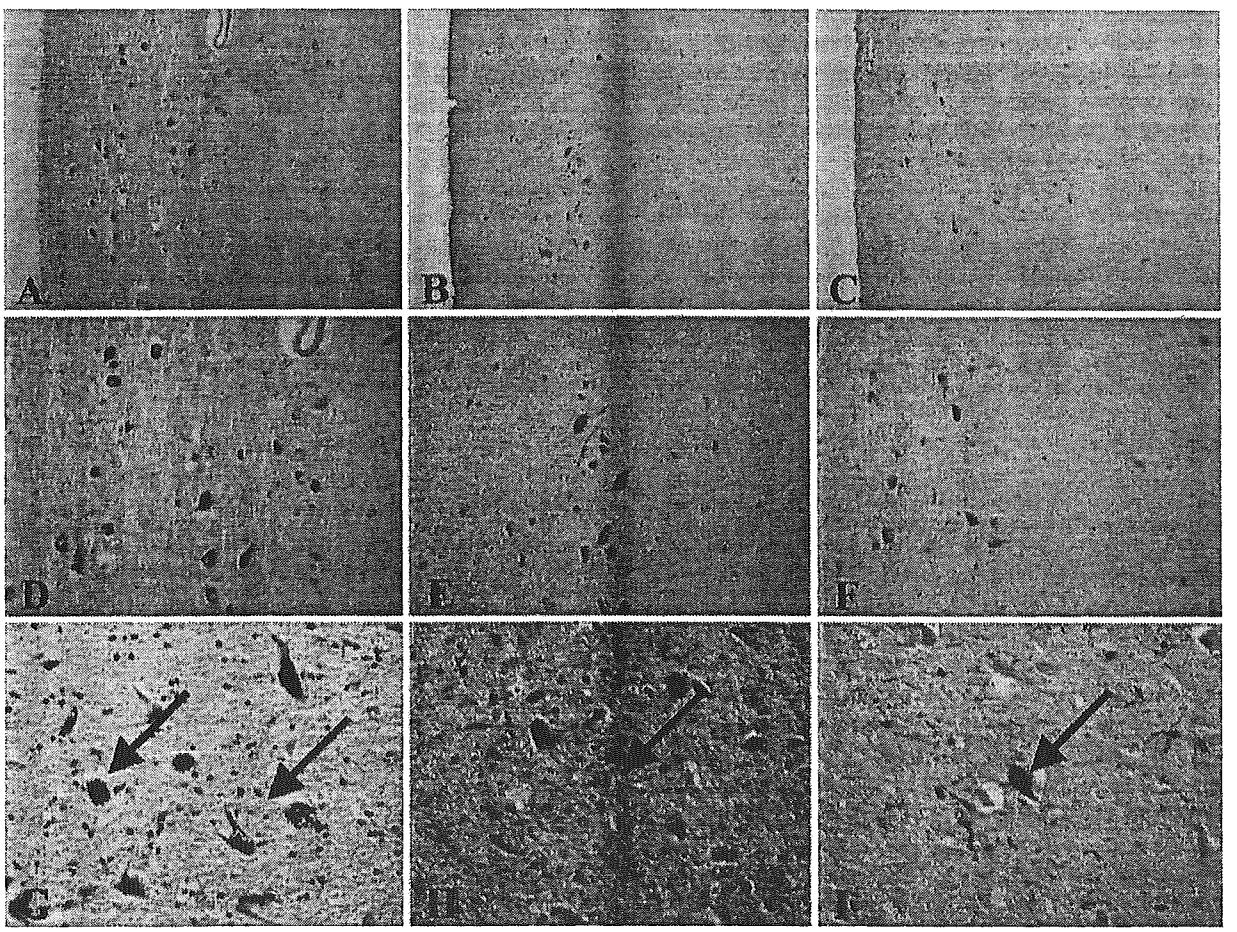

Fig. 1 **a** and **d** ChAT-immunoreactive neurons in the Ch1–2 regions of case 2 (non-demented). **b** and **e** ChAT-immunoreactive neurons in the Ch1–2 regions of case 4 (AD). **c** and **f** ChAT-immunoreactive neurons in the Ch1–2 regions of case 9 (DLB). ChAT immunostainings are shown at a total magnification of 100 times (**a–c**) or 200 times (**d–f**). **g** Neurofibrillary tangle (*NFT*) (*arrows*) in the Ch1–2 regions of the AD brain at a total magnification of 400 times by Gallyas–Braak staining. **h** and **i** Lewy bodies (*arrow*) in the Ch1–2 regions of the DLB brain at a total magnification of 400 times by HE staining and α-synuclein immunostaining

ChAT-immunoreactive neurons in the Ch1 region tend to be ovoid with vertical orientation, while most of those in the Ch2 region are fusiform-to-oval. In addition, the ChAT-immunoreactive neurons appeared to be sparser in the Ch1–2 regions of the DLB brains than in those of the AD and control brains (Fig. 1a–c). On the other hand, the degree of immunostaining was variable, ranging from light to strong in all cases (Fig. 1d–f).

When Alzheimer pathology was examined according to Braak staging [4], the control cases and most of the DLB cases were found to be in Braak stages 1–3 (Table 1). These findings did not fulfill the neuropathologic criteria for definite AD. Moreover, neurofibrillary tangles were observed in the Ch2 region of all the AD cases by using the Gallyas–Braak staining method, but were not found in the Ch2 region of the DLB and control cases (Fig. 1g). On the other hand, Lewy bodies were observed in the Ch1–2 regions of the DLB group (Fig. 1h, i).

ChAT-immunostaining revealed cholinergic neuronal changes in the Ch1–2 regions of the DLB brains. Significant differences among the three groups were found in both the number and the mean surface area of the ChAT-immunoreactive neurons projecting to the hippocampus (each $p < 0.05$, Kruskal–Wallis test). The number of these neurons was significantly reduced in the DLB group compared with the AD and control groups (each $p < 0.05$, Mann–Whitney *U*-test). No significant difference was found in the number of the ChAT-immunoreactive neurons between the AD and control groups, as expected from the previous studies [21, 23] (Fig. 2). On the other hand, when densitometric analysis of ChAT-immunoreactive neurons was performed, the mean surface areas of the AD and DLB groups were significantly reduced compared with the control group (each $p < 0.05$, Mann–Whitney *U*-test). No significant difference was found in the mean surface area of the ChAT-immunoreactive neurons between the AD and DLB groups (Fig. 3).

Discussion

In this study, we found that the cholinergic neurons projecting to the hippocampus were notably degenerated in the DLB group compared with the AD and control groups. However, no significant difference was found in the number of the ChAT-immunoreactive neurons between the AD and control groups, in agreement with the previous reports [21, 23]. Moreover, the mean surface area of ChAT-immunoreactive neurons in the AD and DLB groups was significantly reduced as compared with that in the control group. Based on the fact that atrophy of basal forebrain neurons occurs with the degenerative processes in AD [25, 29], our study showed that cholinergic neurons in the Ch1–2 regions of the AD group were relatively spared in comparison with those of the DLB group. Curiously, a previous volumetry study based on MR imaging supports our results: Brenneis et al. reported that the atrophy of the basal forebrain, including the Ch1–2 regions, of patients with DLB was significantly greater than that of patients with AD [3]. Because Lewy pathology, but not AD pathology, was observed in the Ch1–2 regions of all the DLB cases in the present study, cholinergic neuronal degeneration in the Ch1–2 regions might be specific to the pathogenesis of DLB.

The major cholinergic input to the hippocampus enters the structure via the fimbria-fornix, and the distribution of cholinergic fibers and terminals in the

Table 1 Clinical and pathological data of our cases

	Age (years)	Sex	Brain wt. (g)	Braak stage (NFT)	Duration of Illness	Cause of death
Control (non-demented)						
1	87	F	1015	2	–	Pancreas cancer
2	80	M	1260	1	–	Prostate cancer, heart failure
3	83	F	1160	2	–	Acute cardiomyocarditis
Alzheimer's disease (*AD*)						
4	84	M	1140	5	3	Pneumonia
5	83	F	1040	6	6	Gastric cancer
6	84	F	1070	5	15	Gastric cancer
7	83	M	1110	5	7	Pneumonia
Dementia with Lewy bodies (*DLB*)						
8	47	F	1060	0[a]	4	Heart failure
9	82	M	1150	3	3	Pneumonia
10	79	M	1300	3	3	Pneumonia
11	69	M	1240	3	3	Pneumonia
12	85	F	1010	3	9	Heart failure
13	72	M	1350	1	4	Pneumonia
14	84	M	1200	2	7	Pneumonia
15	82	F	1290	2	4	Pneumonia

[a]No NFT in the brain

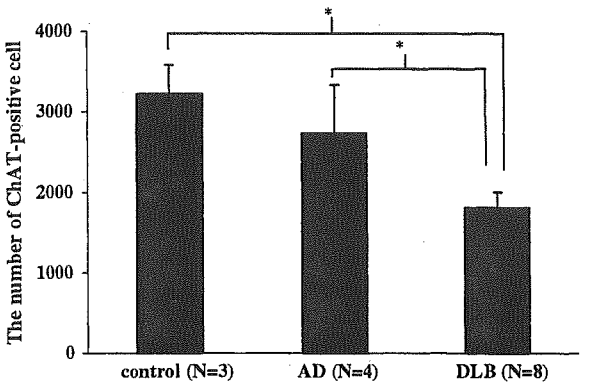

Fig. 2 The number of ChAT-positive neurons projecting to the hippocampus in each group. $*p < 0.05$

hippocampus has been reported [14]. Curiously, a previous study showed that punctate ChAT-immunostaining was conspicuous in the stratum pyramidale of the CA2–3 area, and that the highest density of ChAT-positive terminals was found in the stratum pyramidale and the juxtrapyramidal zone of the stratum oriens [27]. Another immunostaining study revealed that nerve growth factor (NGF), which plays an important role in sustaining and surviving cholinergic neurons, is mainly localized within the CA2–4 area, but is not present in the CA1 or subiculum [24]. On the other hand, Lewy-related neurites in the DLB brains are specific to the CA2–3 area in the hippocampus. In addition, ultrastructural and immunohistochemical studies suggest that these neurites are abnormal axon terminals. These findings lead us to conjecture that the depletion of cholinergic neurons projecting to the hippocampus in the DLB brain can be attributed to the Lewy-related neurites of the CA2–3 area. However, we did not investigate the ChAT-immunoreactivity of Lewy-related neurites in the present study, and thus, further studies will be needed to clarify the origin of Lewy-related neurites in the CA2–3.

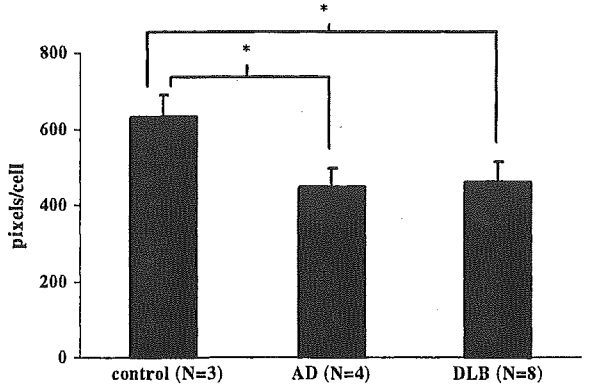

Fig. 3 The mean surface area (pixels/cell) of ChAT-positive neurons in each group. $*p < 0.05$

There have been several animal studies on immunotoxic lesions that specifically damage the cholinergic neurons projecting to the hippocampus. For example, monkeys with damages to the cholinergic neurons projecting to the hippocampus showed impaired performance on visual-spatial conditional learning tasks [28]. Moreover, rats with similar damages to cholinergic neurons showed impaired performance on environment-spatial conditional learning tasks [12]. These results may indicate that cholinergic neurons projecting to the hippocampus participate in certain visual-spatial cognitive impairments specific to DLB patients [5, 20].

Some clinical trials have reported that cholinesterase inhibitors are more effective in DLB patients than in AD patients [13, 30]. Treatment with these agents has positive effects on cognitive impairments, psychiatric symptoms, and global dysfunction. Visual hallucination, which is one of the three core clinical features in DLB, is also improved by cholinesterase inhibitors. From a clinical point of view, the severe depletion of cholinergic neurons projecting to the hippocampus in DLB might provide grounds for pharmacological intervention with cholinesterase inhibitors.

Reference

1. Akatsu H, Takahashi M, Matsukawa N, Ishikawa Y, Kondo N, Sato T, Nakazawa H, Yamada T, Okada H, Yamamoto T, Kosaka K (2002) Subtype analysis of neuropathologically diagnosed patients in a Japanese geriatric hospital. J Neurol Sci 196:63–69
2. Bohnen NI, Kaufer DI, Ivanco LS, Koeppe RA, Davis JG, Mathis CA, Moore RY, DeKosky ST (2003) Cortical cholinergic function is more severely affected in parkinsonian dementia than in Alzheimer disease: an in vivo positron emission tomographic study. Arch Neurol 60:1745–1748
3. Brenneis C, Wenning GK, Egger KE, Schocke M, Trieb T, Seppi K, Marksteiner J, Ransmayr G, Benke T, Poewe W (2004) Basal forebrain atrophy is a distinctive pattern in dementia with Lewy bodies. Neuroreport 15:1711–1714
4. Braak H, Braak E (1991) Neuropathological stageing of Alzheimer-related changes. Acta Neuropathol 82:239–259
5. Collerton D, Burn D, McKeith I, O'Brien J (2003) Systematic review and meta-analysis show that dementia with Lewy bodies is a visual-perceptual and attentional-executive dementia. Dement Geriatr Cogn Disord 16:229–237
6. Dickson DW, Ruan D, Crystal H, Mark MH, Davies P, Kress Y, Yen S-H (1991) Hippocampal degeneration differentiates diffuse Lewy body disease (DLBD) from Alzheimer's disease: light and electron microscopic immunocytochemistry of CA2-3 neurites specific to DLBD. Neurology 41:1402–1409
7. Dickson DW, Schmidt ML, Lee VM-Y, Zhao M-L, Yen S-H, Trojanowski JQ (1994) Immnoreactivity profile of hippocampal CA2/3 neurites in diffuse Lewy body disease. Acta Neuropathol 87:269–276
8. Folstein M, Folstein SE, McHugh PR (1975) Mini-mental state. A practical method for grading the cognitive state of patients for the clinician. J Psychiatr Res 12:189–198
9. Galvin JE, Uryu K, Lee VM-Y, Trojanowski JQ (1999) Axon pathology in Parkinson's disease and Lewy body dementia hippocampus contains α-, β-, and γ-synuclein. Proc Natl Acad Sci USA 96:13450–13455
10. Iraizoz I, Guijarro JL, Gonzalo LM, De Lacalle S (1999) Neuropathological changes in the nucleus basalis correlate with clinical measures of dementia. Acta Neuropathol 98:186–196

11. Iseki E, Li F, Odawara T, Kosaka K (1997) Hippocampal pathology in diffuse Lewy body disease using ubiquitin immunohistochemistry. J Neurol Sci 149:165–169
12. Janisiezka AM, Jackson O III, Firoz EF, Baxter MG (2004) Environment-spatial conditional learning in rats with selective lesions of medial septal cholinergic neurons. Hippocampus 14:265–273
13. Kaufer DI (2004) Pharmacologic treatment expectations in the management of dementia with Lewy bodies. Dement Geriatr Cogn Disord 17:32–39
14. Kitt CA, Mitchell SJ, Delong MR, Wainer BH, Price DL (1987) Fiber pathways of basal forebrain cholinergic neurons in monkeys. Brain Res 406:192–206
15. Kordower JH, Gash DM, Bothwell M, Hersh L, Mufson EJ (1989) Nerve growth factor and choline acetyltransferase remain colocalized in the nucleus basalis (Ch4) of Alzheimer's disease patients. Neurobiol Aging 10:287–294
16. Lippa CF, Smith TW, Perry E (1999) Dementia with Lewy bodies: choline acetyltransferase parallels nucleus basalis pathology. J Neural Transm 106:525–535
17. Marui W, Iseki E, Kato M, Akatsu H, Kosaka K (2004) Pathological entity of dementia with Lewy bodies and its differentiation from Alzheimer's disease. Acta Neuropathol 108:121–128
18. McKeith IG, Galasko D, Kosaka K, Perry EK, Dickson DW, Hansen LA, Salmon DP, Lowe J, Mirra SS, Byrne EJ, Lennox G, Quinn NP, Edwardson JA, Ince PG, Bergeron C, Burns A, Miller BL, Lovestone S, Collerton D, Jansen ENH, Ballard C, de Vos RAI, Wilcock GK, Jellinger KA, Perry RH (1996) Consensus guidelines for the clinical and pathologic diagnosis of dementia with Lewy bodies (DLB). Neurology 47:1113–1124
19. Mesulam M-M, Mufson EJ, Levey AI, Wainer BH (1983) Cholinergic innervation of cortex by the basal forebrain: cytochemistry and cortical connections of the septal area, diagonal band nuclei, nucleus basalis (substantia innominata) and hypothalamus in the rhesus monkey. J Comp Neurol 214:170–197
20. Mori E, Shimomura T, Fujimori M, Hirono N, Imamura T, Hashimoto M, Tanimukai S, Kazui H, Hanihara T (2000) Visuoperceptual impairment in Dementia with Lewy bodies. Arch Neurol 57:489–493
21. Mufson EJ, Bothwell M, Kordower JH (1989) Loss of nerve growth factor receptor-containing neurons in Alzheimer's disease: a quantitative analysis across subregions of the basal forebrain. Exp Neurol 105:221–232
22. Mufson EJ, Bothwell M, Hersh LB, Kordower JH (1989) Nerve growth factor receptor immunoreactive profiles in the normal, aged human basal forebrain: colocalization with cholinergic neurons. J Comp Neurol 285:196–217
23. Mufson EJ, Cochran E, Benzing W, Kordower JH (1993) Galaninergic innervation of the cholinergic vertical limb of the diagonal band (Ch2) and bed nucleus of the stria terminalis in aging, Alzheimer's disease and down's syndrome. Dementia 4:237–250
24. Mufson EJ, Conner JM, Varon S, Kordower JH (1994) Nerve growth factor-like immunoreactive profiles in the primate basal forebrain and hippocampal formation. J Comp Neurol 341:507–519
25. Pearson RCA, Sofroniew MV, Cuello AC, Powell TPS, Eckenstein F, Esiri MM, Wilcock GK (1983) Persistence of cholinergic neurons in the basal nucleus in a brain with senile dementia of the Alzheimer's type demonstrated by immunohistochemical staining for choline acetyltransferase. Brain Res 289:375–379
26. Perry EK, Irving D, Kerwin JM, McKeith IG, Thompson P, Collerton D, Fairbairn AF, Ince PG, Morris CM, Cheng AV, Perry RH (1993) Cholinergic transmitter and neurotrophic activities in Lewy body dementia: similarity to Parkinson's and distinction from Alzheimer disease. Alzheimer Dis Assoc Disord 7:69–79
27. Ransmayr G, Cervera P, Hirsch E, Ruberg M, Hersh LB, Duyckaerts C, Hauw J-J, Delumeau C, Agid Y (1989) Choline acetyltransferase-like immunoreactivity in the hippocampal formation of control subjects and patients with Alzheimer's disease. Neuroscience 32:701–714
28. Ridley RM, Barefoot HC, Maclean CJ, Pugh P, Baker HF (1999) Different effects on learning ability after injection of the cholinergic immunotoxin ME20. 4IgG-saporin into the diagonal band of Broca, basal nucleus of Meynert, or both in monkeys. Behav Neurosci 113:303–315
29. Rinne JO, Paljarvi L, Rinne UK (1987) Neuronal size and density in the nucleus basalis of Meynert in Alzheimer's disease. J Neurol Sci 79:67–76
30. Tiraboschi P, Hansen LA, Alford M, Sabbagh MN, Schoos B, Masliah E, Thal LJ, Corey-Bloom J (2000) Cholinergic dysfunction in disease with Lewy bodies. Neurology 54:407–411
31. The national institute on aging, reagan institute working group on diagnostic criteria for the neuropathological assessment of Alzheimer's disease (1997) Consensus recommendations for the postmortem diagnosis of Alzheimer's disease. Neurobiol Aging 18:S1–S2

Available online at www.sciencedirect.com
SCIENCE DIRECT®
ELSEVIER
Biochemical and Biophysical Research Communications 335 (2005) 631–636
BBRC
www.elsevier.com/locate/ybbrc

Lib, transcriptionally induced in senile plaque-associated astrocytes, promotes glial migration through extracellular matrix

Kazuki Satoh [a,*], Mitsumi Hata [a], Tomoko Shimizu [a], Hiroshi Yokota [b], Hiroyasu Akatsu [c], Takayuki Yamamoto [c], Kenji Kosaka [c], Tatsuo Yamada [d]

[a] *The Fifth Frontier Project, Daiichi Pharmaceutical Co., Ltd., Tokyo 134-8640, Japan*
[b] *Drug Discovery Research Laboratory, Daiichi Pharmaceutical Co., Ltd., Tokyo 134-8640, Japan*
[c] *Choju Medical Institute, Fukushimura Hospital, Aichi 441-8124, Japan*
[d] *Fifth Department of Internal Medicine, Fukuoka University, Fukuoka 814-0180, Japan*

Received 12 July 2005
Available online 10 August 2005

Abstract

In an effort to identify astrocyte-derived molecules that may be intimately associated with progression of Alzheimer's disease (AD), Lib, a type I transmembrane protein belonging to leucine-rich repeat superfamily, has been identified as a distinctly inducible gene, responsive to β-amyloid as well as pro-inflammatory cytokines in astrocytes. To evaluate the roles of Lib in AD, we investigated Lib expression in AD brain. In non-AD brain, Lib mRNA has been detected in neurons but not in quiescent astrocytes. On the contrary, in AD brain, Lib mRNA is expressed in activated astrocytes associated with senile plaques, but not expressed in neurons around lesions. Lib-expressing glioma cells displayed promotion of migration ability through reconstituted extracellular matrix and recombinant Lib protein bound to constituents of extracellular matrix. These observations suggest that Lib may contribute to regulation of cell–matrix adhesion interactions with respect to astrocyte recruitment around senile plaques in AD brain.

Keywords: LRR; mRNA expression; Alzheimer's disease; Cellular migration; Extracellular matrix

Neuropathological changes in the brains from patients with Alzheimer's disease (AD) include loss of neurons, intracellular formation of neurofibrillary tangles, appearance of numerous β-amyloid (Aβ)-containing amyloid plaques, as well as reactive gliosis. Numerous reactive astrocytes observed in lesions are a common feature of an AD brain as well as in many other neurodegenerative disorders. They surround senile plaques and have morphological changes, extending processes into the lesions and producing a variety of inflammatory mediators [1–5]. These observations support the notion that the activated astrocytes in AD lesions have a significant influence on the neighboring neurons and their environment, leading to exacerbation of the disease.

In efforts to identify key molecules from astrocytes intimately involved in the disease, Lib (an LRR protein induced by β-amyloid treatment) was identified as a distinctly inducible gene, responsive to Aβ as well as to pro-inflammatory cytokines in astrocytes [6]. Lib protein is a type I transmembrane protein with an extracellular domain consisting of 15 leucine-rich repeats (LRRs) flanked by both N- and C-terminal cysteine-rich regions that form intramolecular disulfide loops, similar to the extracellular binding motifs of some adhesion proteins and receptors [7–9]. Lib is thought to play a role in inflammatory states via the LRR motif, an ideal structural framework for specific protein–protein and/or protein–matrix interactions including adhesion, target recognition or receptor–ligand binding [6–10].

In this study, the distribution of Lib mRNA expression in AD brain was evaluated to give insight into the

* Corresponding author. Fax: +81 3 5696 8196.
E-mail address: satohj7i@daiichipharm.co.jp (K. Satoh).

0006-291X/$ - see front matter © 2005 Elsevier Inc. All rights reserved.
doi:10.1016/j.bbrc.2005.07.117

pathological involvement of Lib. Based on the observation that Lib is expressed in plaque-associated activated astrocytes, the functional involvement of Lib in glial migration through extracellular matrix (ECM) was analyzed. Although interactions between ECM macromolecules and astrocytes are required in migrating towards and remaining around the AD lesions, molecular mechanisms involved with these events are not well understood. Our results suggest that Lib may participate in astroglial motility around senile plaques in AD brain.

Materials and methods

Brains. The brains were obtained from the brain bank of the Choju Medical Institute of Fukushimura Hospital and protocols used were approved by the Ethics Committee of Fukushimura Hospital. The scientific use of this human material was conducted in accordance with the Declaration of Helsinki and informed consents were obtained from the guardians of the patients. The brains from five neurologically normal control patients in which Alzheimer's disease (AD)-type changes were lacking, and those from five patients with AD were examined. The diagnosis of AD was established using the criteria recommended by the National Institute on Aging [11] and the Consortium to Establish a Registry for Alzheimer's Disease (CERAD) [12]. The ages of the three male and two female neurologically normal controls ranged from 54 to 82 years, and those of the two male and three female patients with AD from 67 to 80 years. In all cases, brains were obtained within 2–13 h after death. Small blocks were dissected from the parietal lobes and stored at −80 °C until used. The frozen samples were thawed and fixed for 2 days in phosphate-buffered 4% paraformaldehyde. They were then transferred to a maintenance solution of 15% sucrose in 0.1 M phosphate buffer, pH 7.4, and kept in the cold until used. Sections were cut on a freezing microtome at 20-μm thickness.

In situ hybridization. Human Lib expression in AD brain tissue was evaluated by in situ hybridization histochemistry. Human Lib cDNA fragments, encompassing nucleotides 1444–1742 of hLib open-reading frame (ORF; Accession No. AB071037), were amplified by PCR and cloned into pCR-Blunt II-TOPO (Invitrogen). A cDNA probe for hLib was constructed by PCR using T7 and SP sequences in the vector as primers. Amplifications were done in 100 μl PCR buffer containing 10 pM primer, 2 nM dNTPs, 200 pM digoxigenin-11-dUTP (Roche), 10 ng template plasmid, and 5 U Ampli-Taq DNA polymerase using a thermal cycler (Perkin-ElmerGeneAmp PCR System 9600). Samples were denatured at 94 °C for 5 min, followed by 30 cycles of amplification for 30 s at 94 °C, for 30 s at 50 °C, and for 30 s at 72 °C. The final extension was at 72 °C for 5 min. Sections were hybridized at 37 °C for 2 days in buffer containing 50% formamide, 4× SSC, 0.2× Denhardt's solution, 21 ng/ml salmon sperm DNA, and 250 ng/ml digoxigenin-11-dUTP labeled and non-labeled PCR DNA probes. After hybridization, sections were rinsed three times in 1× SSC. Hybridization was detected by an enzyme-catalyzed color reaction using the DIG Nucleic Acid Detection kit (Boehringer–Mannheim Biochemica) according to the supplier's instructions. Negative controls were pretreated with RNAase and processed with identical procedures. Other control experiments were done using mixtures of either 10:1 or 1:1 of the digoxigenin-11dUTP-labeled and non-labeled PCR DNA probes. After detection of the mRNA signal for hLib by in situ hybridization, immunohistochemistry [13] was used to characterize the labeled cells using antibody against anti-glial fibrillary acidic protein (GFAP) (1:10,000, rabbit polyclonal, Dako). The sections were mounted on glass slides and the coverslips were sealed with liquid paraffin.

Cell culture and transfection. Human glioma cells were purchased from the American Type Culture Collection. U87MG cells were maintained in Eagle's minimum essential medium (EMEM; Gibco) supplemented with non-essential amino acids (Gibco), pyruvate, and 10% fetal calf serum (FCS; Gibco) at 37 °C under 5% CO_2. H4 cells were cultured in Dulbecco's modified Eagle's medium (DMEM; Gibco) containing 10% FCS. The cells were transfected either with phLib-FLAG plasmid harboring the open-reading frame (ORF) of hLib tagged with a FLAG epitope at the carboxyl terminus or with control empty vector (pCMV-Tag4; Stratagene) using FuGene 6 (Roche). Stably transfected cells expressing hLib and control mock cells were selected with G418 (400 μg/ml; Gibco) for 6 weeks and then obtained as mixed cell lines to avoid clonal variability.

Western blot analysis. Cells were washed with ice-cold phosphate-buffered saline (PBS) and lysed by incubation in lysis buffer (1% NP-40, 150 mM NaCl, 20 mM Hepes, pH 7.5, and complete protease inhibitor cocktail (Roche)) on ice for 30 min. Clarified lysates were obtained by centrifugation (30 min, 15,000*g*, 4 °C). Supernatants were boiled with SDS sample buffer (5 min), separated on a 4–12% sodium dodecyl sulfate–polyacrylamide gel (Novex), and transferred to a polyvinylidene fluoride (PVDF) membrane (NEN). Membranes were immersed for 1 h in blocking solution (5% non-fat dried milk in PBS containing 0.1% Tween 20 (PBS-T)) and probed with a polyclonal antibody raised against hLib (1:2000) in blocking solution overnight at 4 °C. The membranes were washed extensively in PBS-T and incubated with horseradish peroxidase (HRP)-conjugated anti-rabbit IgG antibody (Amersham, 1:3000) in PBS-T at room temperature for 1 h. FLAG-tagged proteins were detected by M2 anti-FLAG antibody (1:2000, Sigma) in blocking solution overnight at 4 °C. Blots were washed and visualized with enhanced chemiluminescence (ECL; Amersham). The actin antibody (Sigma; AC-40) was used as a loading control.

Transmigration analysis. The role of Lib in cellular motility migration through reconstituted extracellular matrix (ECM) was investigated using BioCoat Matrigel 24-well invasion chambers (Becton–Dickinson) according to the supplier's instructions. Cell suspensions (0.5 ml of 5×10^4 cells/ml in 10% FCS-containing medium) were plated onto Matrigel-coated filters in triplicate wells of an invasion chamber. After the 22 h incubation, non-transmigration cells remaining on the upper surface of the filter were removed with a cotton swab and the invasive cells on the under surface were fixed and stained with Diff-Quick staining kit (Kokusai Shiyaku). The cells were photographed at 100× magnification in five predetermined fields and counted.

Blot overlay binding analysis. For production of recombinant hLib protein from sf9 cells (Invitrogen), the extracellular region of hLib (aa 1–529) tagged with His6 at C-terminal was cloned into the pFastBac1 vector (Gibco). The recombinant baculovirus was obtained according to manufacturer's guidelines. Recombinant hLib protein was affinity purified from cultured supernatants of infected sf9 cells using HiTrap Chelating HP (Amersham). Ability of hLib to bind to Matrigel (Becton–Dickinson, 356237), collagen type IV (Becton–Dickinson, 354245), laminin (Becton–Dickinson, 354232), fibronectin (Becton–Dickinson, 354008), aggrecan (Sigma, A1960), and bovine serum albumin (Sigma, A2153) was determined as previously described [14] with slight modifications. Briefly, each macromolecule was spotted onto a PVDF membrane at 5 μg and 0.5 μg/spot. The membrane was incubated with blocking solution at room temperature for 2 h and then incubated with recombinant hLib protein (1 μg/ml) in blocking solution for 16 h at 4 °C. The membrane was incubated with anti-hLib polyclonal antibody (1:1000) for 16 h at 4 °C, followed by extensive washing, incubation with HRP-conjugated anti-rabbit IgG antibody (1:2000; Amersham), and detection with ECL (Amersham).

Results

Lib expression in activated astrocytes adjacent to senile plaques of Alzheimer's disease brain

To evaluate pathological involvement of Lib in AD, localization of hLib gene transcripts was evaluated in cerebral cortex sections from the patients by in situ hybridization analysis. As shown in Fig. 1A, mRNA for hLib was expressed in only neurons, but not in astrocytes in age-matched non-AD cortex sections. In AD brain sections, there appeared areas where hLib mRNA expression was not observed in neurons (Fig. 1B, lower central part) and these areas are thought to be damaged. In these 'neuron-negative' areas, hLib mRNA was detected in some cells surrounding the non-specifically stained senile plaques (Fig. 1C). Immunohistochemistry using an anti-GFAP antibody revealed that these hLib mRNA-positive cells were reactive astrocytes. As shown in Fig. 1D, GFAP-positive astrocytes directly surrounding and extending their processes toward non-specifically faintly stained senile plaques expressed hLib mRNA. Review of five AD brain sections indicated that approximately half of the reactive astrocytes around senile plaques were positive for hLib mRNA expression. Control hybridization sections which were incubated without the DNA probe or with a 1:1 mixture of the digoxigenin-11dUTP-labeled and non-labeled PCR DNA probe were negative. When a 10:1 mixture of the digoxigenin-11dUTP-labeled and non-labeled PCR DNA probe was used, only a weak signal could be detected (data not shown).

Lib promotes glial migration ability through ECM

Cell surface LRR proteins appear to have abilities to interact with extracellular proteins and/or matrixes [7–9]. The observation that Lib is expressed in reactive astrocytes around AD senile plaques (Fig. 1) prompted us to evaluate a role of Lib in cellular migration through ECM. The hLib expression plasmid, harboring hLib ORF with FLAG epitope tag at the C-terminus, was introduced into U87MG and H4 human glial cell lines. Human Lib expression from transfected cells was verified by Western blot analyses using an antibody raised against hLib and M2 anti-FLAG antibody. As shown in Fig. 2A, hLib protein was expressed in established cell lines, while hLib expression was undetectable in both parental wild type and empty vector control lines. The bands observed near 64 kDa are thought to correspond to immature molecules before complete glycosylation [10]. These cells were examined by migration analysis using Matrigel invasion chambers. Human Lib expression promoted migration through Matrigel in both transfected

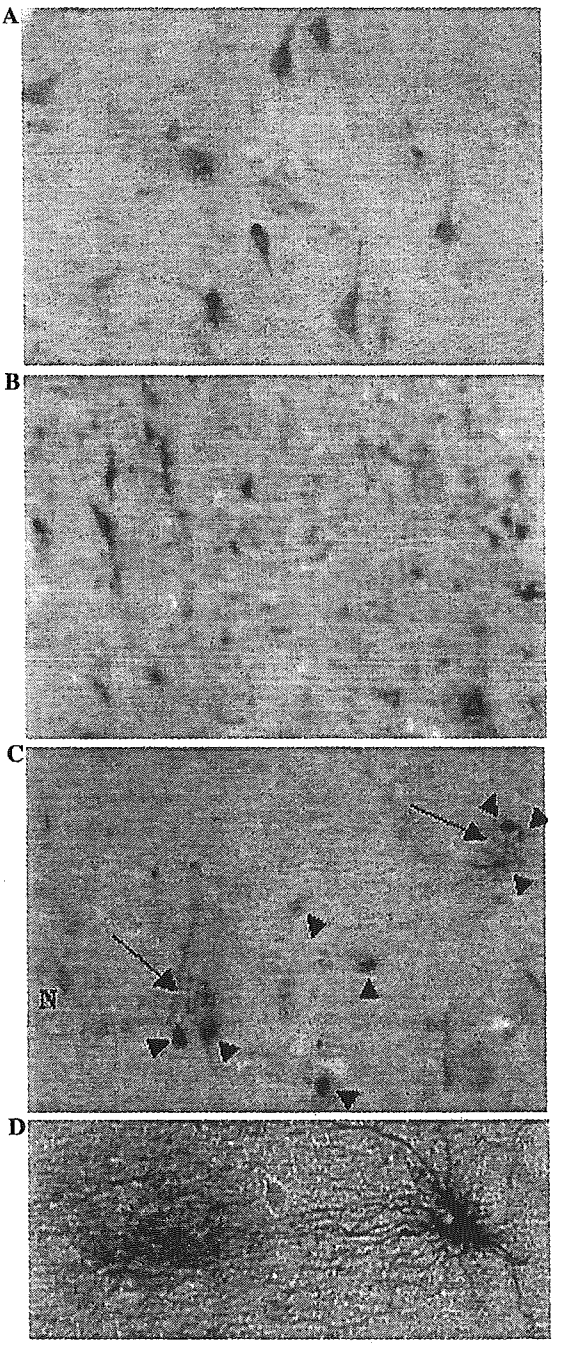

Fig. 1. In situ localization of hLib mRNA in non-AD (A) and AD brain sections (B–D). (A) Positive signals for hLib mRNA were seen in neurons in non-AD cerebral cortex. (B) In AD brain, neurons positive for hLib mRNA expression were observed, similar to non-AD brain. However, unlike non-AD brain, areas devoid of hLib mRNA expression in neurons were observed (lower central part). (C) In an area where hLib mRNA-positive neurons were not seen, signals for hLib mRNA were seen in several other non-neuronal cells (arrowheads). Some positive cells surrounding non-specifically stained senile plaques (arrows) were observed. A neuron with damaged morphology was faintly stained (N). Non-specific staining was seen in some vessels. (D) In situ hybridization histochemistry for hLib mRNA (blue-black) followed by immunohistochemistry with anti-GFAP antibody (brown) in AD brain. Human Lib mRNA-positive cell, that directly surrounded and extended processes toward the non-specifically faintly stained senile plaque, also expressed GFAP. (A–C) 185×; (D) 256×.

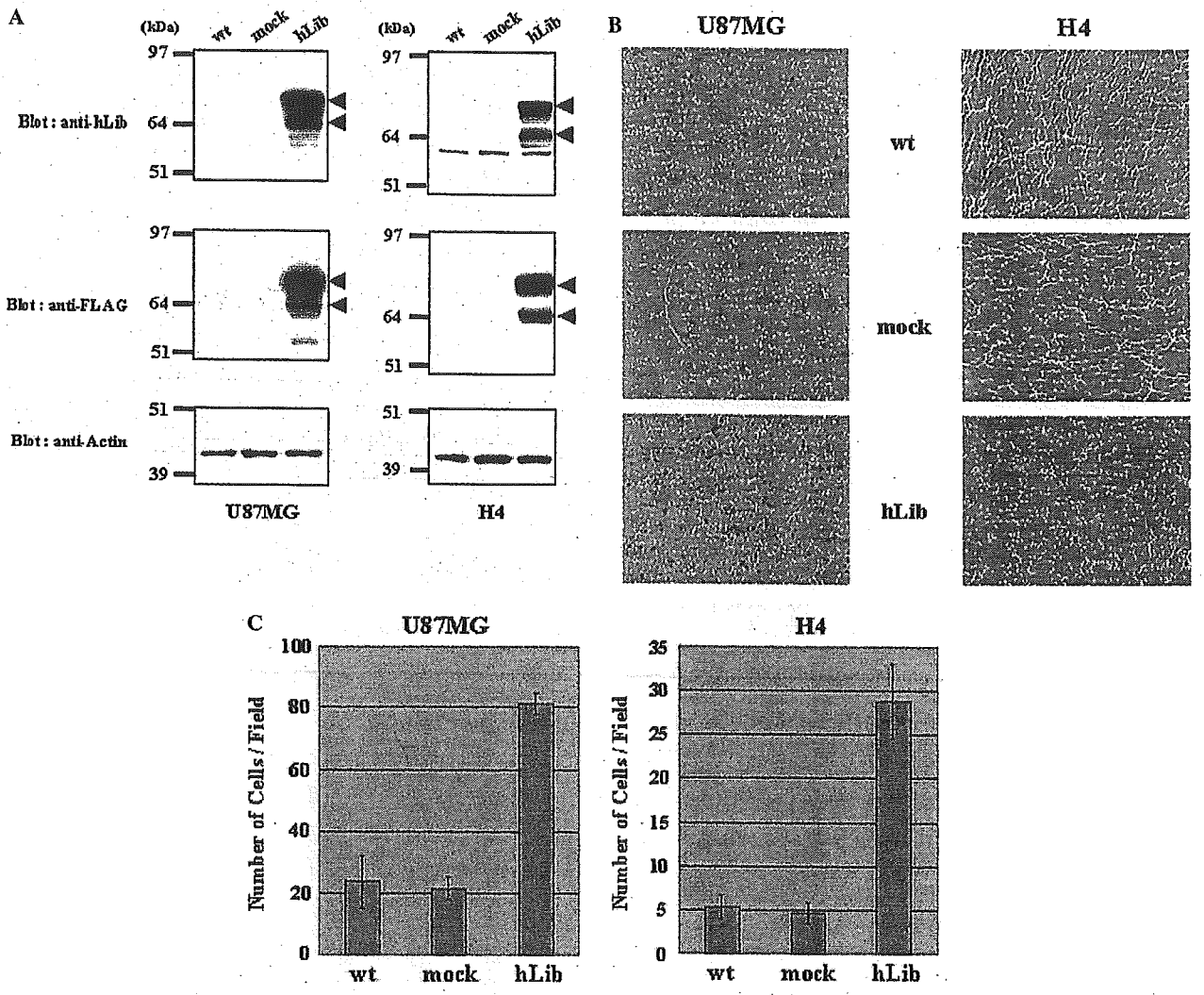

Fig. 2. Acceleration of cell migration by hLib expression. (A) Expression of hLib in transfected U87MG (left panels) or H4 (right panels) cells were detected by Western blot analysis using polyclonal antibody raised against hLib (top panels) or M2 anti-FLAG antibody (middle panels). Anti-hLib antibody reacted with hLib gene products (arrowheads) only in hLib-transfected cells (hLib) and not in parental wild type (wt) or empty vector control (mock) cells. Specific bands were detected similarly with M2 anti-FLAG antibody. Blotting with actin antibody was used as a loading control (bottom panels). (B) Migration analyses using Matrigel chambers. Parental wild type (wt), empty vector control (mock), and hLib-expressing cells (hLib) were plated on top of Matrigel-coated 8-μm filters. After 22 h, cells migrating through the filter were stained, visualized, and counted. (C) Graphical representation of average number of migration through Matrigel at 22 h. Results are means ± SEM from three independent experiments.

U87MG and H4 cells (Figs. 2B and C). These results demonstrate that Lib appears to be a LRR membrane protein that is involved in cell–ECM interactions important for glial migration.

Lib binds to extracellular matrix

Blot overlay assays were used to assess Lib binding to Matrigel and ECM macromolecules using affinity-purified extracellular region (aa 1–529) of hLib protein (Fig. 3A). Lib bound to fibronectin preferentially relative to Matrigel, collagen type IV or laminin, with minimal to no binding to aggrecan and BSA (Fig. 3B). Decreased dose of blotted macromolecules resulted in reduction of signal intensities.

Discussion

In the present study, we evaluated hLib mRNA expression in AD brains in comparison with age-matched non-AD brains. Human Lib mRNA was detected in activated astrocytes around senile plaques in AD and in these areas the signals for hLib mRNA in neurons were not observed. Similar to results from in vitro studies on rLib in rat astrocytes [6], hLib is also a distinctly inducible gene in human astrocytes in vivo, because signals for hLib mRNA were detected in reactive astrocytes in AD brain, but not in quiescent astrocytes in non-AD brain nor in lesion-free areas of AD brains. In contrast, neurons express hLib mRNA in non-AD brains and in lesion-free areas of AD

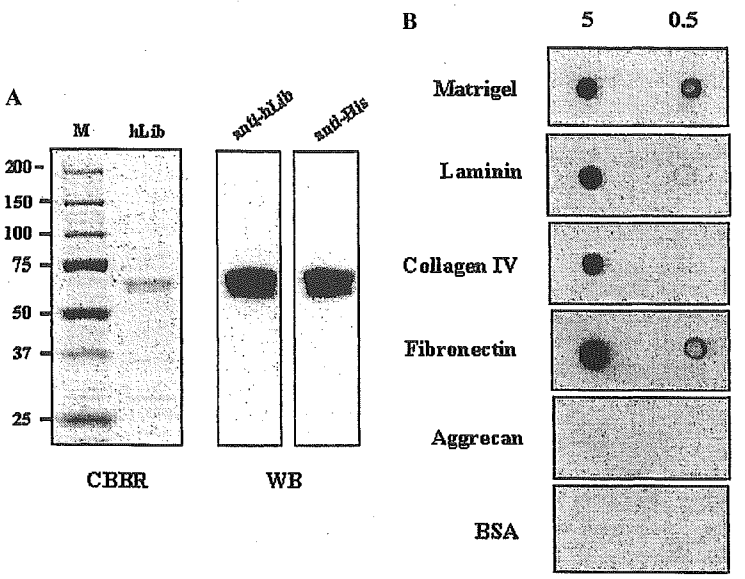

Fig. 3. Binding of hLib to ECM molecules. (A) Recombinant extracellular region of hLib was affinity purified from cultured supernatants of infected sf9 cells, followed by electrophoresis, and staining with CBBR250 (CBBR, left panel) (M, molecular size marker) or Western blotting with anti-hLib antibody (WB, right panel). (B) Matrigel, laminin, collagen type IV, fibronectin, aggrecan, and BSA were immobilized on PVDF membrane at 5 μg and 0.5 μg/spot. The PVDF membrane was then incubated with recombinant hLib, excessively washed, and immuno-detected using anti-hLib antibody.

brains. These results suggest that hLib expression may be required for maintenance of homeostasis in neuronal activities, although it is not clear whether loss of hLib mRNA in neurons of AD brains is caused by cellular death or loss of homeostasis in diseased neurons. It is also possible that Lib may play different roles in astrocytes and neurons, because some LRR proteins are involved in the regulation of neurite guidance and synapse formation [15–17].

Based on the presence of the LRR motif, Lib has been thought to play a role in specific cell–cell and/or cell–matrix interactions in astrocytes. The finding, that hLib mRNA is transcriptionally induced in activated astrocytes of AD brains, prompted us to evaluate the possibility that hLib may participate in the accumulation of astrocytes around senile plaques in cell–matrix interactions. The current data show that glial cells expressing hLib display accelerated migration through Matrigel, a reconstituted ECM. This effect on cellular motility is consistent with an other study showing reduction of cellular migration after suppressing hLib expression in a tumor cell line [18]. In addition, hLib protein demonstrates binding to some ECM constituents with some preferentiality, similar to other LRR proteins [19–21]. These results suggest that Lib may contribute to the regulation of cell–matrix adhesion interactions with respect to astrocyte recruitment around senile plaques.

In our previous study, ADAMTS-4, an ECM-degrading enzyme, was screened out from the same Aβ-treated astrocyte cDNA library [22]. Other studies have demonstrated that matrix metalloprotease (MMP) activities responsible for degradation of ECM are higher in brains from AD patients than in controls, and that these ECM degradation enzymes are derived from astrocytes [23,24]. To investigate the possibility that these reported MMP (MMP-2, MMP-3, and MMP-9) activities were transcriptionally up-regulated in hLib-expressing glial cells, their mRNA expression levels were evaluated by reverse transcriptase PCR (RT-PCR). However, they were not increased in hLib-transfected cells compared to parental or control mock cells in both U87MG and H4 cells (data not shown).

Astrocyte recruitment toward lesions is thought to be dependent on chemotactic molecules, such as MCP-1, originated from the core of senile plaques in lesions [25], accompanied with recognition of, adhesion to, and reducing integrity of ECM. Lib appears to participate in these steps by specific protein–protein and/or matrix interactions. Further investigation into Lib molecular mechanisms may provide additional insight into astroglial motility around lesions, suggesting novel therapeutic strategies.

Acknowledgments

We greatly appreciate Seiji Takahara and Hidetoshi Tsuzaki for technical support and advice, and Yasuhide Hirota for helpful discussion and encouragement.

References

[1] C.J. Pike, B.J. Cummings, C.W. Cotman, Early association of reactive astrocytes with senile plaques in Alzheimer's disease, Exp. Neurol. 132 (1995) 172–179.

[2] E.G. McGeer, P.L. McGeer, The inflammatory response system of brain: implications for therapy of Alzheimer and other neurodegenerative diseases, Brain Res. 21 (1995) 195–218.

[3] R.E. Mrak, J.G. Sheng, W.S. Griffin, Glial cytokines in Alzheimer's disease: review and pathogenic implications, Hum. Pathol. 26 (1995) 816–823.

[4] D.W. Dickson, The pathogenesis of senile plaques, J. Neuropathol. Exp. Neurol. 56 (1997) 321–339.

[5] M. Johnstone, A.J. Gearing, K.M. Miller, A central role for astrocytes in the inflammatory response to beta-amyloid; chemokines, cytokines and reactive oxygen species are produced, J. Neuroimmunol. 93 (1999) 182–193.

[6] K. Satoh, M. Hata, H. Yokota, A novel member of the leucine-rich repeat superfamily induced in rat astrocytes by beta-amyloid, Biochem. Biophys. Res. Commun. 290 (2002) 756–762.

[7] B. Kobe, J. Deisenhofer, The leucine-rich repeat: a versatile binding motif, Trends Biochem. Sci. 19 (1994) 415–421.

[8] S.G. Buchanan, N.J. Gay, Structural and functional diversity in the leucine-rich repeat family of proteins, Prog. Biophys. Mol. Biol. 65 (1996) 1–44.

[9] B. Kobe, A.V. Kajava, The leucine-rich repeat as a protein recognition motif, Curr. Opin. Struct. Biol. 11 (2001) 725–732.

[10] K. Satoh, M. Hata, H. Yokota, High Lib mRNA expression in breast carcinomas, DNA Res. 11 (2004) 199–203.

[11] Z.S. Khachaturian, Diagnosis of Alzheimer's disease, Arch. Neurol. 42 (1985) 1097–1105.

[12] S.S. Mirra, A. Heyman, D. McKeel, S.M. Sumi, B.J. Crain, L.M. Brownlee, F.S. Vogel, J.P. Hughes, G. van Belle, L. Berg, The Consortium to Establish a Registry for Alzheimer's Disease (CERAD). Part II. Standardization of the neuropathologic assessment of Alzheimer's disease, Neurology 41 (1991) 479–486.

[13] T. Yamada, Y. Tsujioka, J. Taguchi, M. Takahashi, Y. Tsuboi, T. Shimomura, White matter astrocytes produce hepatocyte growth factor activator inhibitor in human brain tissues, Exp. Neurol. 153 (1998) 60–64.

[14] V.M. Paralkar, B.S. Weeks, Y.M. Yu, H.K. Kleinman, A.H. Reddi, Recombinant human bone morphogenetic protein 2B stimulates PC12 cell differentiation: potentiation and binding to type IV collagen, J. Cell Biol. 119 (1992) 1721–1728.

[15] E. Shishido, M. Takeichi, A. Nose, *Drosophila* synapse formation: regulation by transmembrane protein with Leu-rich repeats, CAPRICIOUS, Science 280 (1998) 2118–2121.

[16] J.A. Howitt, N.J. Clout, E. Hohenester, Binding site for Robo receptors revealed by dissection of the leucine-rich repeat region of Slit, EMBO J. 23 (2004) 4406–4412.

[17] J. Kuja-Panula, M. Kiiltomaki, T. Yamashiro, A. Rouhiainen, H. Rauvala, AMIGO, a transmembrane protein implicated in axon tract development, defines a novel protein family with leucine-rich repeats, J. Cell Biol. 160 (2003) 963–973.

[18] P.A. Reynolds, G.A. Smolen, R.E. Palmer, D. Sgroi, V. Yajnik, W.L. Gerald, D.A. Haber, Identification of a DNA-binding site and transcriptional target for the EWS-WT1(+KTS) oncoprotein, Genes Dev. 17 (2003) 2094–2107.

[19] R.V. Iozzo, The biology of the small leucine-rich proteoglycans. Functional network of interactive proteins, J. Biol. Chem. 274 (1999) 18843–18846.

[20] K. Saito, T. Tanaka, H. Kanda, Y. Ebisuno, D. Izawa, S. Kawamoto, K. Okubo, M. Miyasaka, Gene expression profiling of mucosal addressin cell adhesion molecule-1+ high endothelial venule cells (HEV) and identification of a leucine-rich HEV glycoprotein as a HEV marker, J. Immunol. 168 (2002) 1050–1059.

[21] A.N. Malhas, R.A. Abuknesha, R.G. Price, Interaction of the leucine-rich repeats of polycystin-1 with extracellular matrix proteins: possible role in cell proliferation, J. Am. Soc. Nephrol. 13 (2002) 19–26.

[22] K. Satoh, N. Suzuki, H. Yokota, ADAMTS-4 (a disintegrin and metalloproteinase with thrombospondin motifs) is transcriptionally induced in beta-amyloid treated rat astrocytes, Neurosci. Lett. 289 (2000) 177–180.

[23] A. Lukes, S. Mun-Bryce, M. Lukes, G.A. Rosenberg, Extracellular matrix degradation by metalloproteinases and central nervous system diseases, Mol. Neurobiol. 19 (1999) 267–284.

[24] S. Deb, P.E. Gottschall, Increased production of matrix metalloproteinases in enriched astrocyte and mixed hippocampal cultures treated with beta-amyloid peptides, J. Neurochem. 66 (1996) 1641–1647.

[25] T. Wyss-Coray, J.D. Loike, T.C. Brionne, E. Lu, R. Anankov, F. Yan, S.C. Silverstein, J. Husemann, Adult mouse astrocytes degrade amyloid-beta in vitro and in situ, Nat. Med. 9 (2003) 453–457.

Brief Communication

Quinoline and Benzimidazole Derivatives: Candidate Probes for *In Vivo* Imaging of Tau Pathology in Alzheimer's Disease

Nobuyuki Okamura,[1,2] Takahiro Suemoto,[1] Shozo Furumoto,[3] Masako Suzuki,[1] Hiroshi Shimadzu,[1] Hiroyasu Akatsu,[4] Takayuki Yamamoto,[4] Hironori Fujiwara,[5] Miyako Nemoto,[6] Masahiro Maruyama,[6] Hiroyuki Arai,[5] Kazuhiko Yanai,[2] Tohru Sawada,[1] and Yukitsuka Kudo[1,3]

[1]BF Research Institute, Osaka 541-0045, Japan, [2]Department of Pharmacology, Tohoku University Graduate School of Medicine, Sendai 980-8575, Japan, [3]Tohoku University Biomedical Engineering Research Organization, Sendai 980-8575, Japan, [4]Choju Medical Institute, Fukushimura Hospital, Toyohashi 441-8124, Japan, and Departments of [5]Geriatric and Complementary Medicine and [6]Geriatric and Respiratory Medicine, Tohoku University Graduate School of Medicine, Sendai 980-8574, Japan

Neurofibrillary tangles (NFTs), neuropil threads, and neuritic elements of senile plaques predominantly comprise hyperphosphorylated tau protein and represent pathological characteristics of Alzheimer's disease (AD). These lesions occur before the presentation of clinical symptoms and correlate with the severity of dementia. *In vivo* detection of these lesions would thus prove useful for preclinical diagnosis of AD and for tracking disease progression. The present study introduces three novel compounds, 4-[2-(2-benzoimidazolyl)ethenyl]-*N*,*N*-diethylbenzenamine (BF-126), 2-[(4-methylamino)phenyl]quinoline (BF-158), and 2-(4-aminophenyl)quinoline (BF-170), as candidate probes for *in vivo* imaging of tau pathology in the AD brain. When solutions of these compounds are injected intravenously into normal mice, these agents exhibit excellent brain uptake and rapid clearance from normal brain tissue. These compounds display relatively lower binding affinity to β-amyloid fibrils and higher binding affinity to tau fibrils, compared with previously reported probe BF-168. In neuropathological examination using AD brain sections, BF-126, BF-158, and BF-170 clearly visualize NFTs, neuropil threads, and paired helical filament-type neuritis. Autoradiography using ^{11}C-labeled BF-158 further demonstrated labeling of NFTs in AD brain sections. These findings suggest the potential usefulness of quinoline and benzimidazole derivatives for *in vivo* imaging of tau pathology in AD.

Key words: imaging; neuropathology; Aβ peptide; tau; neurofibrillary tangles; paired helical filaments

Introduction

The deposition of senile plaques (SPs) and neurofibrillary tangles (NFTs) represents a pathological hallmark of Alzheimer's disease (AD). Definitive diagnosis of AD relies on the postmortem assessment of these pathological changes. SPs are extracellular deposits containing β-amyloid (Aβ) peptide cleaved from a longer amyloid precursor protein to produce a 40–43 aa peptide. NFTs comprise bundles of paired helical filaments (PHFs) that result from the abnormal aggregation of tau protein (Lee et al., 1991). PHFs accumulate in the neuronal cytoplasm and form NFT with age. Initial lesions of NFTs occur in the transentorhinal cortex, followed by involvement of the entorhinal cortex and hippocampus, progressing to the neocortex (Braak and Braak, 1991). Severity of neurofibrillary pathology correlates with severity of cognitive impairment (Dickson, 1997). However, these pathological changes can be observed in elderly individuals with normal cognition. The pathological process of AD must therefore begin before the presentation of the clinical symptoms of dementia (Price and Morris, 1999). Recent drug development has been aimed at preventing the accumulation of SPs and NFTs in presymptomatic AD patients. The ability to measure levels of these lesions in the living human brain is thus desirable for presymptomatic diagnosis of AD.

Many attempts have been made to visualize AD-specific pathological changes in the living brain (Nordberg, 2004). Currently, the most practical methods for this purpose are to measure the distribution of intravenously administered radiotracers that selectively bind to SPs or NFTs using positron emission tomography (PET) or single photon emission computed tomography. Such radiotracers require sufficient permeability to the blood–brain barrier (BBB). Several researchers have focused on developing lipophilic radiotracers for imaging AD-specific pathology (Shoghi-Jadid et al., 2002; Klunk et al., 2004; Kung et al., 2004; Mathis et al., 2004; Okamura et al., 2004a). To obtain a better understanding of the pathophysiology of AD, individual evaluation of the distributions of Aβ pathology and tau pathology is desirable. However, no surrogate markers exist that allow evaluation of the severity of neurofibrillary pathology in AD brains, because of the difficulty in developing an NFT-specific imaging probe (Small et al., 2002).

We screened >2000 small molecules to develop novel agents

Received May 2, 2005; revised Sept. 26, 2005; accepted Sept. 27, 2005.

This study was supported by the Organization for Pharmaceutical Safety and Research of Japan, the New Energy and Industrial Technology Development Organization, and the Novartis Foundation for Gerontological Research.

Correspondence should be addressed to Yukitsuka Kudo, Tohoku University Biomedical Engineering Research Organization, 2-1, Seiryo-machi, Aoba-ku, Sendai 980-8575, Japan. E-mail: kudoyk@tubero.tohoku.ac.jp.

DOI:10.1523/JNEUROSCI.1738-05.2005

 0270-6474/05/2510857-06$15.00/0

for use in PET with a high affinity for SPs and NFTs. This process has identified novel quinoline and benzimidazole derivatives with a preference to bind NFTs rather than SPs and readily cross the BBB. The present study evaluated whether these compounds may offer a good indicator of tau pathology in AD patients.

Materials and Methods

Preparation of BF compounds. Three novel compounds, 4-[2-(2-benzoimidazolyl)ethenyl]-*N*,*N*-diethylbenzenamine *p*-toluenesulfonate (BF-126), 2-[(4-methylamino)phenyl]quinoline (BF-158), and 2-(4-aminophenyl)quinoline (BF-170), were originally designed by us and custom-synthesized by Tanabe R&D Service (Osaka, Japan) (see Fig. 1*A*). [^{11}C]BF-158 was synthesized from N-Boc-protected BF-170 and [^{11}C]methyl triflate (see Fig. 1*B*). Briefly, to a solution of N-Boc-protected BF-170 and NaH in dry acetone was bubbled thorough [^{11}C]methyl triflate at room temperature, followed by heating at 80°C for 1 min. The reaction was then acidified with a dioxane solution of hydrochloric acids and heated for an additional 5 min. After neutralizing the reaction with sodium phosphate buffer, the crude mixture was purified with semipreparative reverse-phase HPLC to give [^{11}C]BF-158 with a radiochemical purity of >95% and a specific activity of 11–15 GBq/μmol at the end of synthesis. Isolated [^{11}C]BF-158 was solubilized into 40% ethanol solution for *in vitro* autoradiography of AD brain sections and saline with polysorbate 80 for *in vivo* brain-uptake study using normal mice.

Biodistribution of BF compounds in normal mice. Brain uptake after intravenous injection of BF-126 and BF-170 in mice was analyzed using HPLC with a fluorescence detector, as described previously (Okamura et al., 2004b). Briefly, each compound (1 mg/kg), dissolved in diluted HCl, was administered into the tail vein of male Institute of Cancer Research (ICR) mice (7 weeks of age; body weight, 30–40 g; $n = 3$). At 2 and 30 min after the injection of compounds, the brain was removed. Brain homogenates were centrifuged at 14,000 rpm for 10 min, and the supernatant was used for extraction. The mobile phase was 20 mM phosphate buffer, pH 6.5, and acetonitrile at a ratio of 2:3 for BF-126 and 1:1 for BF-170, at a flow rate of 1 ml/min. An FS-8020 fluorescence detector (Tosoh, Tokyo, Japan) was operated at excitation/emission wavelengths of 420/525 nm for BF-126 and 280/500 nm for BF-170. Brain uptake of BF-158 was measured using ^{11}C-labeled compound. [^{11}C]BF-158 (2.6–3.3 MBq) was administered into the tail vein of ICR mice ($n = 12$; male; average weight, 24 g). The mice were then killed by decapitation at 2, 10, 30, and 60 min after injection. The brains were removed and weighted, and the radioactivity was counted with an automatic γ-counter (Wizard 1480; PerkinElmer Wallac, Turku, Finland). The percentage injected dose per gram (%ID/g) was calculated by comparison of tissue count to tissue weight. Each %ID/g value is an average ± SEM of three separate experiments.

In vitro *binding assays.* The dissociation constant (K_d) and maximum specific binding of BF-180 were determined as described previously (Okamura et al., 2004a). For inhibition studies, binding studies were performed using aggregates of synthetic Aβ1–42 (Peptide Institute, Osaka, Japan). A mixture containing 50 μl of BF-126, BF-158, and BF-170, 50 μl of 0.05 nM [^{125}I]BF-180, 100 μl of 100 nM Aβ1–42, and 800 μl of 8% ethanol was incubated at room temperature for 4 h. The mixture was then filtered, and filters containing bound ^{125}I ligand were counted using the γ-counter. Values for half-maximal inhibitory concentration (IC_{50}) were determined from displacement curves of three independent experiments using GraphPad Prism software (GraphPad Software, San Diego, CA), and those for the inhibition constant (K_i) were determined using the Cheng–Prusoff equation.

In addition, fluorescence assay of the compounds with Aβ1–42 and tau fibrils was performed. The 412 aa isoform of human tau was expressed from cDNA clone htau46 in *Escherichia coli* and purified as described previously (Hasegawa et al., 1998). Aβ1–42 (0.2 mg/ml; Peptide Institute) in 50 mM potassium phosphate buffer, pH 7.4, was incubated at 37°C for 72 h with gentle shaking. Tau protein (1 mg/ml) was incubated in the presence of 0.1 mg/ml heparin for 72 h with continuous shaking. Fluorescence spectra of a mixture of the same amount of 0.2 mg/ml Aβ1–42 or 0.1 mg/ml tau and 10, 3, 1, 0.3, 0.1, 0.03, and 0.01 μM concentrations of each compound were measured using a microplate spectrofluorometer (Gemini XS; Molecular Devices, Sunnyvale, CA). Optimal excitation wavelength for the mixture of four BF compounds and Aβ1–42 or tau fibrils were determined. Then, EC_{50} values (effective concentrations to achieve 50% maximal fluorescence intensity at optimal excitation wavelength) were calculated using GraphPad Prism. All measurements were performed in duplicate.

Measurement of octanol/water partition coefficients. 1-Octanol (Wako Pure Chemicals, Osaka, Japan) and PBS was saturated with PBS and 1-octanol before use, respectively. Test compounds were dissolved in 1-octanol and shaken with equal amounts of PBS for 30 min at room temperature. After centrifugation at 2000 per min for 15 min, the absorbency of 1-octanol layer was measured at the peak wavelength of the absorbance spectrum of each compound using a microplate reader (Molecular Devices Spectra Max 190). The octanol/water partition coefficients were determined by comparing the absorbency with that before shaking with PBS. Each data point was performed in duplicate.

Neuropathological staining. Stainability of tested compounds were examined using postmortem brain tissues from cases of autopsy-confirmed AD (78-year-old woman), Pick's disease (75-year-old woman), and progressive supranuclear palsy (PSP) (78-year-old man). Brain sections were obtained from Fukushimura Hospital. Experiments were performed in accordance with the regulations of the ethics committee of the BF Research Institute. Serial sections (6 μm thick) from paraffin-embedded blocks of hippocampus were used for staining. After deparaffinization, quenching of autofluorescence was performed as described previously (Okamura et al., 2004a). Quenched tissue sections were immersed in 100 μM compound or 0.125% thioflavin-S solution containing 50% ethanol for 10 min. Finally, sections were dipped briefly into water, rinsed in PBS for 60 min, coverslipped with FluorSave Reagent (Calbiochem, Darmstadt, Germany), and examined using a Nikon (Tokyo, Japan) Eclipse microscope equipped with a violet filter (excitation, 380–420 nm; dichroic mirror, 430 nm; barrier filter, 450 nm) and a blue filter (excitation, 450–490 nm; dichroic mirror, 505 nm; barrier filter, 520 nm). For the comparison of stainability between BF compounds and thioflavin-S, a blue–violet filter (excitation, 400–440 nm; dichroic mirror, 455 nm; long-pass filter, 470 nm) was used. Staining was also performed in AD brain sections pretreated with 90% formic acid for 5 min. Sections stained with BF compounds were subsequently immunostained with AT8 anti-tau antibody (diluted 1:20; Innogenetics, Ghent, Belgium) to detect tau pathology. An adjacent section was also immunostained with 6F/3D anti-Aβ antibody (diluted 1:50; Dako, High Wycombe, UK). Sections were placed in blocking buffer for 30 min and then incubated at 4°C with primary antibodies for 18 h (AT8) or 1 h (6F/3D). After washing, sections were incubated with biotinylated anti-mouse IgG (Wako Pure Chemicals, Tokyo, Japan) for 60 min, followed by Texas Red-conjugated avidin (Vector Laboratories, Burlingame, CA) for 60 min. After coverslipping, sections were examined using a Nikon Eclipse microscope with a green filter set (excitation, 510–560 nm; dichroic mirror, 575 nm; barrier filter, 590 nm).

In vitro *autoradiography.* A 6-μm-thick section from paraffin-embedded blocks of hippocampus was used for autoradiographic study. After deparaffinization, the section was labeled using 4.7 MBq/ml of [^{11}C]BF-158 at room temperature for 10 min, and then washed briefly with H_2O and 50% ethanol. After drying, the labeled section was exposed to a BAS-III imaging plate (Fujifilm, Tokyo, Japan) for 1 h. Autoradiographic images were obtained using a BAS-5000 phosphorimaging instrument (Fujifilm). Adjacent brain sections were immunostained with anti-tau antibody (AT8) and anti-Aβ antibody (6F/3D), as described previously (Okamura et al., 2004a).

Results

We investigated whether tested compounds would enter the brain in amounts sufficient for *in vivo* brain imaging using PET (Table 1, Fig. 1*C*). The octanol/water partition coefficients of BF-126, BF-158, BF-168, and BF-170 were 12.5, 47.4, 62.6, and 70.3, respectively. These values indicate that these compounds were highly lipophilic. High uptake of these compounds was ap-

Table 1. Octanol/water partition coefficients, brain uptakes at 2 and 30 min after injection in normal mice, K_i values for Aβ 1–42 fibrils, EC_{50} values for Aβ 1–42, and tau fibrils from fluorescence assay of the compounds

	Octanol/water partition coefficient	Brain uptakes (%ID/g)		K_i values for Aβ fibrils (nM)	Fluorescence assay	
		2 min	30 min		EC_{50} for Aβ fibrils (nM)	EC_{50} for τ fibrils (nM)
BF-126	12.5	7.2 ± 0.49	0.16 ± 0.030	1.2 ± 0.68	1280 ± 1.64	583 ± 2.07
BF-158	47.4	11.3 ± 0.81	3.1 ± 0.61	>5000	659 ± 2.04	399 ± 2.41
BF-170	70.3	9.1 ± 1.2	0.25 ± 0.027	>5000	786 ± 1.79	221 ± 2.31
BF-168	62.6	3.9 ± 0.22[a]	1.6 ± 0.0071[a]	6.4 ± 1.0[a]	346 ± 2.21	1010 ± 1.72

Brain uptake and EC_{50} values are shown as the mean ± SEM. K_i values for Aβ fibrils are shown as the mean ± SD.

[a]From Okamura et al., 2004a.

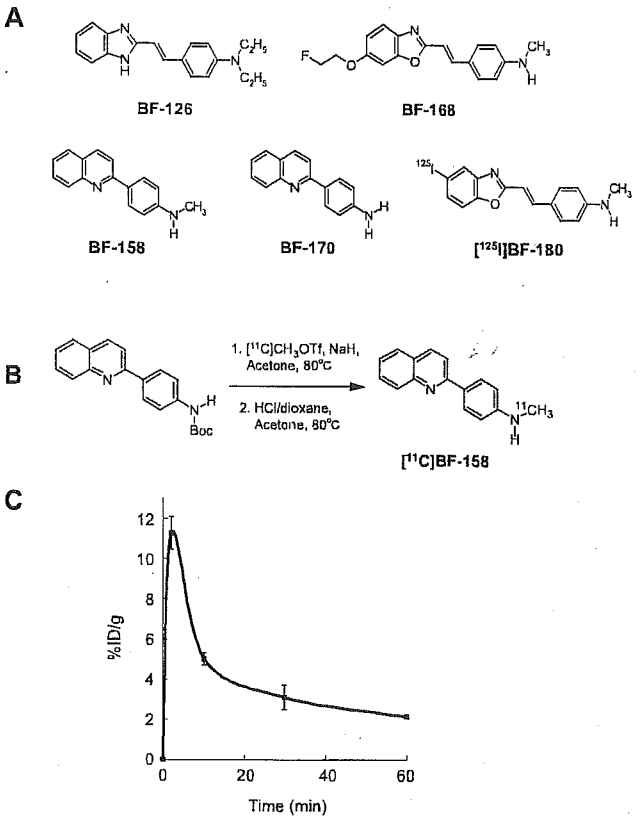

Figure 1. *A*, Chemical structures of BF-126, BF-158, BF-168, BF-170, and [^{125}I]BF-180. *B*, Radiolabeling of BF-158. *C*, The %ID/g obtained in the brains of mice after intravenous administration of [^{11}C]BF-158.

parent in the brain after intravenous administration of each compound, with 7.2%ID/g for BF-126 and 9.1%ID/g for BF-170 at 2 min. These values were higher than those reported previously for compound BF-168 (Okamura et al., 2004a). In addition, brain uptake at 30 min after injection was 0.16%ID/g for BF-126 and 0.25%ID/g for BF-170. Brain uptake of BF-158 was measured using ^{11}C-labeled compound. Brain uptake at 2, 10, 30, and 60 min after intravenous injection of [^{11}C]BF-158 was 11.3 ± 0.81, 5.0 ± 0.31, 3.1 ± 0.61, and 2.1 ± 0.097%ID/g, respectively (Fig. 1*C*). *In vitro* binding of tested compounds to Aβ was examined using synthetic Aβ fibrils. In competitive binding assays with ^{125}I-labeled styrylbenzoxazole compound BF-180, BF-126 displayed high binding affinity to Aβ1–42 fibrils, comparable with BF-168. In contrast, K_i for BF-158 and BF-170 was >5000 nM, suggesting a difference in binding sites between quinoline derivatives and benzoxazole derivatives (Table 1). In the fluorescence binding assay of the mixture of tested compounds and Aβ1–42 fibrils, EC_{50} value was lowest in BF-168, suggesting higher affinity to Aβ compared with the other agents. In contrast, in the assay of the mixture of compounds with tau fibrils, EC_{50} values of BF-170, BF-158, and BF-126 was lower than that of BF-168, suggesting relatively higher binding affinity to tau fibrils.

Subsequently, neuropathological staining was performed using AD brain samples to examine the *in vitro* binding characteristics of tested compounds for AD pathology. BF-126, BF-158, and BF-170 clearly stained NFTs and neuropil threads in the hippocampal section of AD brain (Fig. 2*A–C*). In the comparison with tau immunostaining in the same sections, binding of these compounds with tau pathology was confirmed. In contrast, SPs were faintly stained with BF-126, BF-158, and BF-170, as opposed to clear staining of SPs with thioflavin-S (Fig. 2*A–C*). We further investigated the stainability of neuritic changes using these compounds and BF-168. BF-168 clearly visualized both the central core and peripheral zone of core plaques under violet and blue filters (Fig. 2*D*). The staining pattern for BF-168 did not coincide with that for tau immunostaining in the same section but closely resembled Aβ immunostaining in the adjacent section (Fig. 2*D*). In contrast, BF-126, BF-158, and BF-170 predominantly stained neuritic elements under a blue filter and coincided well with tau immunostaining (Fig. 2*E–G*). Under a violet filter, the central core and peripheral halo were barely visible. These findings suggest that BF-126, BF-158, and BF-170 prefer to bind to PHF-type neurites rather than Aβ fibrils. Pretreatment with formic acid eliminated the staining of NFTs with BF-170 (Fig. 2*H*, *I*), BF-158, and BF-126 (data not shown), suggesting that both compounds recognize the β-sheet structure of NFTs rather than monomeric tau protein. To investigate whether these compounds detect neuropathological lesions in non-AD tauopathy, staining was performed in brain sections from Pick's disease and PSP patients. As a result, BF-126, BF-170, and BF-158 (data not shown) were unable to identify Pick bodies (Fig. 2*J*), globose tangles (Fig. 2*K*), and glial pathology in PSP brain (data not shown).

Finally, *in vitro* autoradiography using [^{11}C]BF-158 was performed in AD brain section. Accumulation of tracer was observed primarily in the gray matter region of the brain. The distribution of labeling with [^{11}C]BF-158 correlated well with tau immunostaining in the adjacent section (Fig. 3*A*, *B*). In particular, high levels of tracer accumulation were observed in NFT-rich brain regions (Fig. 3*D*, *E*, arrows). This finding indicates the binding of [^{11}C]BF-158 for NFTs in the AD brain.

Discussion

Although the present research did not confirm whether the studied compounds can visualize tau pathology in the living brain, the results strongly suggest that quinoline and benzimidazole derivatives represent potential candidates for an *in vivo* tau-imaging agent in AD patients. Requirements for the ideal tau-imaging probe include the following: (1) high BBB and cell membrane permeability; (2) rapid clearance from normal brain tissue; (3) high affinity for NFTs, neuropil threads, and PHF-type neurites; and (4) low nonspecific binding. Our results indicate that BF-126, BF-158, and BF-170 display sufficient BBB permeability for use as PET imaging tracers. Permeability of the neuronal membrane represents another important factor for *in vivo* imaging of intracellular tau aggregates (Small et al., 2002). High lipophilicity

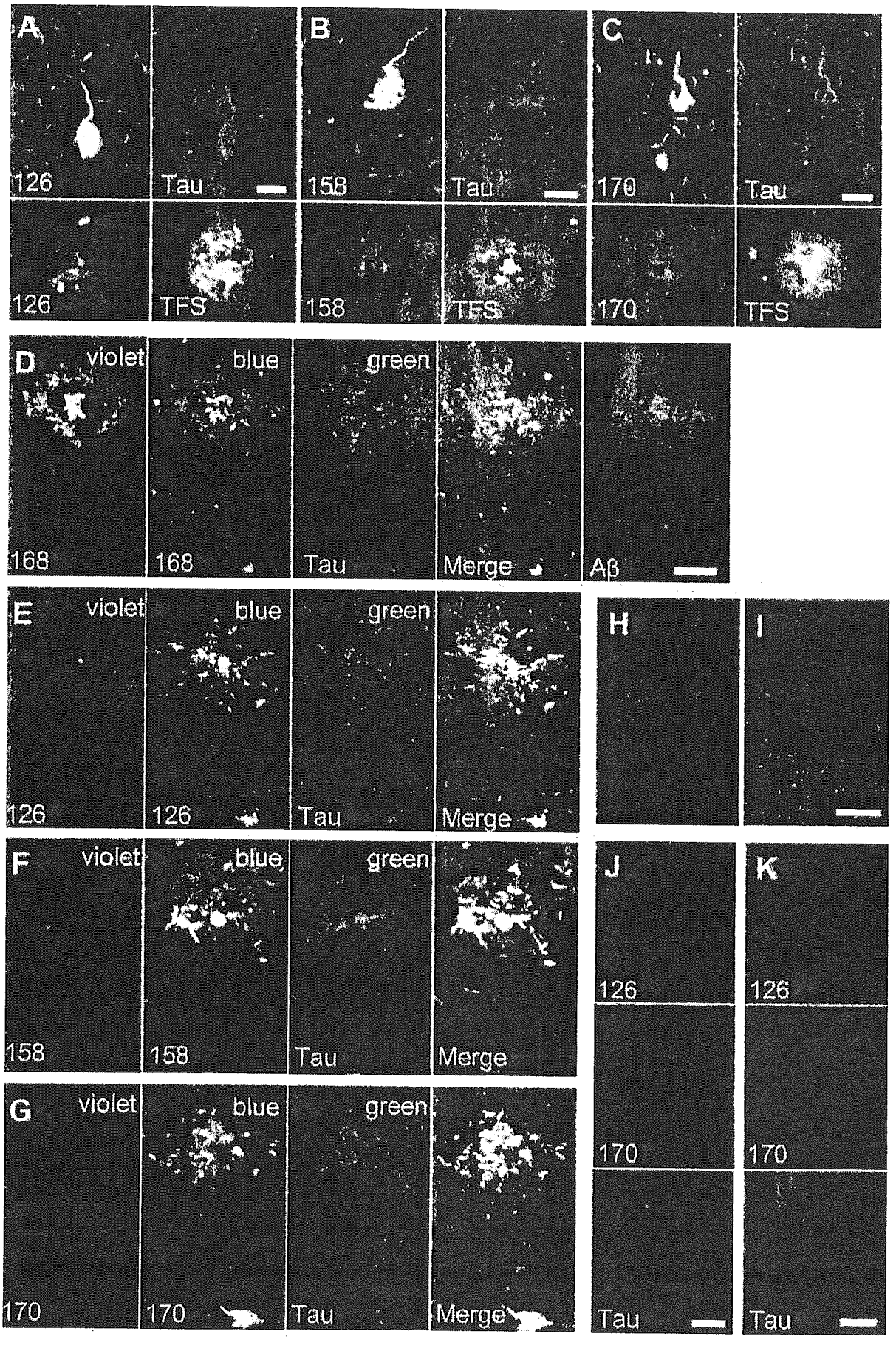
A
126
Tau
126
TFS
B
158
Tau
158
TFS
C
170
Tau
170
TFS
D
violet
blue
green
168
168
Tau
Merge
Aβ
E
violet
blue
green
126
126
Tau
Merge
F
violet
blue
green
158
158
Tau
Merge
G
violet
blue
green
170
170
Tau
Merge
H
I
J
126
170
Tau
K
126
170
Tau